Climate Dynamics
https://doi.org/10.1007/s00382-024-07226-x

Sub-seasonal to seasonal drivers of regional marine heatwaves around Australia

Catherine H. Gregory[1,2] · Neil J. Holbrook[1,2] · Andrew G. Marshall[2,3,4] · Claire M. Spillman[2,5]

Received: 9 November 2023 / Accepted: 31 March 2024

Abstract
As marine heatwaves (MHWs) become more intense and longer lasting due to global warming, understanding the drivers and impacts of these events is crucial for effective marine resource management. This study investigates the influence of El Niño Southern Oscillation (ENSO), the Indian Ocean Dipole (IOD), Southern Annular Mode (SAM), Sub-Tropical Ridge High (STRH), and Madden Julian Oscillation (MJO) on sea surface temperature (SST) anomalies and MHWs around Australia. The aim of this research is to improve our understanding of the drivers of MHWs on sub-seasonal to seasonal (S2S) timescales, which bridges the gap between short-term weather and interannual to long-term climate variability. By analysing SST anomalies and MHWs characteristics during specific driver phases, a simple MHW hazard index is developed. Our findings support previous research indicating that La Niña plays a role in driving MHWs off the coast of Western Australia and reveals a previously unrecognised connection between ocean warming off Queensland and Tasman Sea low-pressure systems associated with the negative phase of the STRH. Our research emphasizes the importance of considering multiple drivers and their compounding effects on MHWs by showing significant changes to typical La Niña MHW patterns with the additional influence of the MJO. By considering drivers acting in the S2S timescale, forecasts can more accurately capture the timing, intensity, and spatial extent of MHW events within a season. These improved forecasts can enhance the ability of marine managers to adapt and allocate resources based on evolving climate conditions, enabling effective implementation of harm minimisation strategies.

1 Introduction

Prolonged and discrete warm ocean temperature extremes, also known as marine heatwaves (MHWs), have increased in frequency and intensity in the past century (Oliver et al. 2018a), leading to a range of ecosystem consequences (Smale et al. 2019; Smith et al. 2021). Australia, with its diverse ocean habitats and one of the world's largest economic exclusion zones, faces significant threats from these extreme events. To effectively manage marine resources, including mitigation of the impacts of MHWs, it is crucial to have early warning systems in place. For these efforts to be successful, the availability of reliable and timely forecasts is paramount. These forecasts serve to provide managers with insight as to the conditions of the upcoming season to support their decision making process (Spillman and Hobday 2014). While long-term decisions such as establishing marine protected areas (Game et al. 2008), selecting target species for fisheries (Caputi et al. 2019), and aiding the recovery of vulnerable ecosystems (Arias-Ortiz et al. 2018) are made on the interannual to decadal time scale, sub-seasonal to seasonal (S2S) forecasts are vital for equipping managers with the necessary insights to make informed shorter term decisions (White et al. 2022). These S2S forecasts are usually in the range of 1–2 weeks to several months, bridging the gap between short-term weather forecasts and longer-term climate projections (Vitart et al. 2017).

Predictions of extreme events can be improved by understanding their connection to modes of climate variability. El Niño–Southern Oscillation (ENSO) is the leading source of seasonal climate variability globally (Wallace et al. 1998;

✉ Catherine H. Gregory
catherine.gregory@utas.edu.au

1 Institute for Marine and Antarctic Studies, University of Tasmania, Hobart, TAS, Australia

2 Australian Research Council Centre of Excellence for Climate Extremes, University of Tasmania, Hobart, TAS, Australia

3 University of Southern Queensland, Toowoomba, QLD, Australia

4 Bureau of Meteorology, Hobart, TAS, Australia

5 Bureau of Meteorology, Melbourne, VIC, Australia

Published online: 19 April 2024

Lenssen et al. 2020) and has been shown to enhance or suppress the likelihood of MHWs around the world, including Australia (Holbrook et al. 2019, 2020). The negative phase of ENSO, La Niña, is associated with an increase in the likelihood of MHWs off the west coast of Australia, known as 'Ningaloo Niño' events (Pearce et al. 2011; Marshall et al. 2015; Xu et al. 2018; Tozuka et al. 2021). While the positive phase of ENSO, El Niño, is linked to dry and warm conditions in the Australian tropical region (Allan and Pariwono 1990) leading to MHWs in the northern region (Benthuysen et al. 2018) and in the Great Barrier Reef (GBR) (McGowan and Theobald 2017; Huang et al. 2024). The Indian Ocean Dipole (IOD) is another important source of seasonal climate variability in Australia (Luo et al. 2010), with the strongest influence occurring during the austral winter (Saji et al. 1999). The negative phase of the IOD has been linked to MHWs in the northern Australian region (Oliver et al. 2018b), while recent research has shown that the positive IOD may be a useful predictor of increased MHW likelihood off Western Australia up to 20 months in advance (Wang et al. 2023). When combined with an El Niño event, the positive phase of the IOD has also been shown to promote atmospheric conditions, including reduced cloud cover, that favours the development of MHWs in the GBR (Benthuysen et al. 2021).

While there is the potential for skilful prediction of ENSO up to one year in advance (Wang et al. 2012) and the IOD up to six months in advance (Zhao et al. 2019), it is important to note that several other climate modes, which are influential on the shorter S2S timescale, ranging from weeks to months, often have limited predictability. The Southern Annular Mode (SAM), for example, describes the latitudinal positioning of the westerly winds in the mid- to high-latitudes of the southern hemisphere (Gong and Wang 1999). During the negative phase of SAM, these westerly winds are seen to contract towards the equator, which has been linked to increased rainfall in eastern Australia (Speer et al. 2011; Min et al. 2013), while the positive SAM phase shows an expansion of these winds to the south. This southward expansion has also been linked to a multi-decadal poleward extension of the East Australian Current (EAC) (Cai et al. 2005; Roemmich et al. 2007) and the positioning and persistence of enhanced downward air-sea heat fluxes, increasing the occurrence of MHWs in the Tasman Sea region (Gregory et al. 2023).

Other short-term atmospheric drivers of anomalous heat exchange into the ocean include persistent anti-cyclones over the Tasman Sea, which have been seen to transport dry, hot air from the interior desert region of Australia southward (Hudson et al. 2011). As these high-pressure systems are located within the vicinity of the subtropical ridge, Marshall et al. (2014) labelled this phenomenon the Subtropical Ridge High (STRH) and developed an index to show that the STRH contributed to increased heating over Australia during all seasons.

Lastly, the Madden Julian Oscillation (MJO), which is the primary mode of influence on tropical weather at the subseasonal timescale (Madden and Julian 1971), has been shown to alter ocean temperatures through changes to surface heat fluxes (Weller and Anderson 1996; Hendon et al. 1998). It possesses a distinct seasonal nature and is easily distinguishable as a slow, eastward moving pattern of atmospheric circulation and deep convection along the equator associated with cloud and rainfall, with a period of propagation around 30 to 80 days (Hendon and Salby 1994). It is described by its strength (amplitude) and the central position of the convective energy (phase). Its convective centre develops over the Indian Ocean (Phases 2–3) before crossing the maritime continent (Phases 4–5), weakening over the Pacific Ocean (Phases 6–7) before eventually dissipating east of the International Dateline (Phases 8 and 1) (Oliver and Thompson 2010). The influence of the MJO on tropical winds and weather patterns has been shown to impact SST variability on the northwest shelf (Marshall and Hendon 2014; Huang and Feng 2021) and in the GBR (Benthuysen et al. 2018).

When considering the impacts of these drivers, it is important to note that the climate modes themselves are often correlated at some level. For example, ENSO and the IOD are strongly correlated, with less than a third of all IOD events occurring independently from ENSO (Loschnigg et al. 2003; Stuecker et al. 2017). Correlations between drivers can also be useful to improve the potential predictability of the drivers themselves. The predictability of SAM, for example, is generally considered low, at only several weeks. However, due to its strong connection with eastern Pacific La Niña and the southern stratospheric polar vortex during the austral warm seasons, models are able to skillfully predict the seasonal variation of SAM in early summer at least one season in advance (Lim et al. 2021).

The key aim of this paper is to provide a broad analysis of how each of these climate modes influence SST variability and the occurrences, or lack thereof, of MHWs in Australian waters. We also consider the relative importance of compounding drivers and their combined influence on ocean temperature variability. The dynamics of these interactions are complex and sometimes complicated, and so we focus on creating the groundwork from which further research can be undertaken to explore these complexities in more detail.

From here, the paper is organized as follows. Section 2, Data and Methods, includes detailed descriptions of all the processes used for the analysis. Section 3 presents our results, where we show composite maps of oceanic and atmospheric anomalies and levels of MHW hazard for each of the drivers, separated by season. In this section we also present a case study to explore the compounding impacts of multiple drivers by showing La Niña impressions that are modulated by the MJO. Finally, Section 4 provides a summary and discussion.

2 Material and methods

2.1 Data

All analysis was performed over the time period 1982–2022. SST data used in this study were from the National Oceanic and Atmospheric Administration (NOAA) Optimum Interpolation Sea Surface Temperature V2.1 (OISSTv2.1) dataset. These 0.25° gridded global SST data are from high-resolution infrared and microwave satellites blended with in-situ observational data from ships and buoys and comprise daily SSTs from 1982 to the present day (Reynolds et al. 2007; Banzon et al. 2016; Huang et al. 2021).

The daily atmospheric data were taken from the National Centre for Environmental Prediction/National Centre for Atmospheric Research (NCEP/NCAR) Reanalysis 2 product. These data were generated using a forecast model that assimilates observational data (Kanamitsu et al. 2002) and, with a relatively coarse spatial grid of 2.5 degrees, is well suited for analysis of large scale processes (Dufek et al. 2008). Variables from the NCEP/NCAR reanalysis used in this study include mean sea level pressure (MSLP) to calculate the SAM and STRH indices, zonal wind data to calculate the MJO index, and the meridional wind fields to show anomalous wind patterns. Outgoing longwave radiation (OLR) data used to calculate the MJO index were taken from NOAA's OLR dataset estimated from polar-orbiting satellites and interpolated to include global spatial coverage on a daily timescale (Liebmann and Smith 1996).

For our heat budget and Ekman transport analysis, we used model output from Bluelink ReANalysis (BRAN) 2020 (Chamberlain et al. 2021) which incorporates observations into an eddy-resolving, near-global ocean circulation model, the Ocean Forecasting Australia Model (OFAM) v3 (Oke et al. 2013). This model is forced by atmospheric fluxes from the Japanese Meteorological Agency 55-year reanalysis (JRA-55) (Kobayashi et al. 2015). Ocean variables are available on a daily timescale at 0.1° resolution.

2.2 Calculation of climate indices

2.2.1 El Niño Southern-Oscillation (ENSO) index

The phase of ENSO was determined using the Oceanic Niño Index (ONI). Using a three month running mean of SST anomalies derived from the OISSTv2.1 dataset in the Niño 3.4 region (5°S—5°N, 170°W-120°W), an El Niño state is detected with a period of at least five consecutive months with SST anomalies $> +0.5$ °C, and a La Niña state detected when SST anomalies < -0.5 °C for a period of at least five consecutive months, and all other periods are considered neutral (Barnston 1997).

The daily ENSO index, used to assess the significant correlations with other drivers, was calculated as the daily SST anomalies (temperature deviations from the mean, calculated using the full daily climatology from 1982–2022), averaged over the Niño 3.4 region (Philander 1983).

2.2.2 Indian Ocean Dipole (IOD) index

The phases of the IOD were determined from the differences between SST values, from OISSTv2.1 dataset, in the western Indian Ocean (between 10°S-10°N and 50°E-70°E) and the tropical south-eastern Indian Ocean (between 10°S-0° and 90°E-110°E). The positive phase shows higher temperatures in the western Indian Ocean and cooler temperatures around Indonesia in the east (Saji et al. 1999). The IOD is considered to be in the positive phase when this difference is $> +0.4$ °C, and in the negative phase when this difference is < -0.4 °C for at least eight consecutive weeks, with all other times considered as neutral (Saji et al. 1999).

2.2.3 Southern Annular Mode (SAM) index

The daily SAM index was calculated by projecting daily MSLP anomalies, from NCEP/NCAR Reanalysis 2, onto the principal component (PC) time series of the leading empirical orthogonal function (EOF) of observed monthly MSLP anomalies between 25°S and 75°S (see Marshall et al. 2014). SAM positive events are identified when the index is one standard deviation, or greater, above the mean and SAM negative events when the index is at least one standard deviation below the mean. Anything in between is characterised as SAM neutral. While there is more variability in the SAM index using daily data, the general spatial structure of the mode does not differ from one generated using monthly values.

2.2.4 Subtropical Ridge High (STRH) index

The STRH index was devised by Marshall et al. (2014) to describe the persistent high pressure blocking systems over the Tasman Sea located within the region of the subtropical ridge. The index is calculated using area averaged MSLP data, from NCEP/NCAR Reanalysis 2, in the region of 150°E-165°E, $y°S \pm 7.5°$ (where y is the latitudinal centre of the subtropical ridge, which varies monthly from the northernmost extent of 27.5°S in August to southernmost of 40°S in February). The positive phase is determined when the index is greater than one standard deviation above the mean, and the negative phase when the index is less than one standard deviation below the mean.

2.2.5 Madden Julian Oscillation (MJO) index

The MJO is distinct from the other climate modes discussed here as it is not described by a positive, negative, and neutral state, but rather by the geographical location of its center of convection (phase) and the strength of its convective energy

(amplitude). The phase and amplitude of the MJO are determined by the leading pair of EOFs from equatorially-averaged (15°S-15°N) fields of 200 hPa and 850 hPa zonal winds and OLR, which are used to compute the Real-time Multivariate MJO (RMM) index (Wheeler and Hendon 2004). The pair of PCs that go with the leading EOFs are referred to as RMM1 and RMM2, and effectively describe the evolution of the MJO along the equator. The MJO is considered to be 'in phase' when the amplitude is greater than 1 and 'out of phase' when the amplitude is less than 1.

To determine the relationship between the phases of the MJO with other drivers, we also calculated each of the phases of the MJO as its own index, following the same method used by Virts and Wallace (2014) and Wang and Hendon (2020).

Figure 1 shows a 3D schematic summary of these drivers, based on the figure by McKay et al. (2023), with the addition of the EAC and the Leeuwin Current, two poleward flowing warm-water boundary currents that we also discuss in our analysis. There are also many other regional currents that can influence MHW occurrences such as the Holloway Current in the Northwest shelf region (Maggiorano et al. 2021) and the North Queensland Current (Huang et al. 2024).

2.3 Calculation of MHW metrics

To calculate MHW metrics we followed the methodology of Hobday et al. (2016), who defined a MHW occurrence when ocean temperature exceeds the 90th percentile relative to daily climatological values for at least five consecutive days. We calculated MHW statistics in the Australian region (0°—50°S, 100°E—180°) from NOAA OISSTv2.1 data from 1982–2022. Where a MHW occurs, the intensity (i.e., the difference between the observed temperature and the climatological mean), was recorded at each grid point. (note: the absence of a MHW event has an intensity of 0).

2.4 MHW hazard index

Here, we created a simple MHW hazard index by considering the increased weekly heat stress that a region is exposed to during each of the phases of the climate modes (drivers) in each season. First, we summed the daily MHW intensity at each grid point for each week. We then composited these weekly intensities based on the phases of the weekly climate mode indices and separated by season. Finally, we removed the average seasonal weekly cumulative intensity (far right column Fig. 2), which is dominated by the west Australian and Tasman Sea regions in all seasons.

The MHW hazard index developed here shows the difference between the average weekly cumulative intensity from the seasonal mean at each grid cell for each driver. By removing this seasonal mean we can more accurately show the change to the hazard level associated with each of the drivers, rather than from general SST variability. When the value is < -1.5°C, we say the MHW hazard level is very low. When the value is between -0.5°C and -1.5°C, it is seen as lower than average. When it is between -0.5°C and 0.5°C, we consider there is no effect. When it is between + 0.5°C and + 1.5°C, it is seen as higher than average. When between + 1.5°C and + 2.5°C, it is seen as very high. And finally, when it is > + 2.5°C, we classify it as extreme.

2.5 Average oceanic and atmospheric states during phases of climate modes

Our study area encompasses the broader Australian region bounded by latitudes 0°—50°S and longitudes 100°E—180°. Figure 2 provides an overview of the study region, with the top

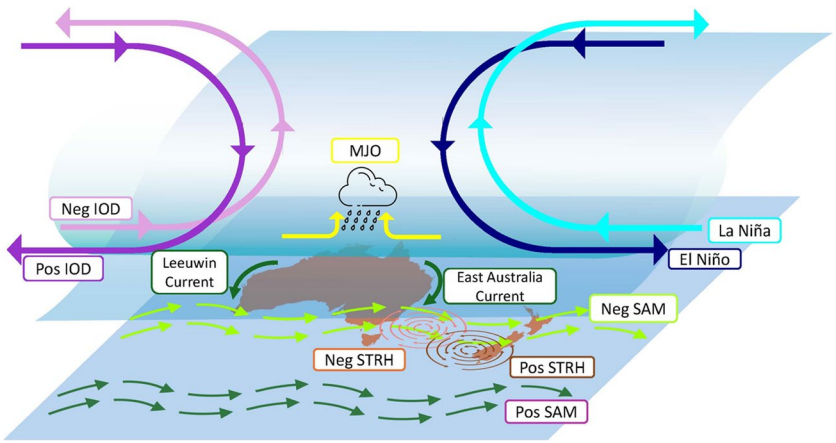

Fig. 1 Schematic representation of the key drivers of MHWs in the Australian region, focusing on subseasonal to seasonal (S2S) timescales. The dominant factors include ENSO in the Pacific Ocean, the IOD in the Indian Ocean, the SAM in the Southern Ocean, the MJO in the tropics, and the STRH over the Tasman Sea. Major ocean currents in the region are the Leeuwin Current, which carries warm water along the west coast, and the East Australian Current (EAC), responsible for transporting warm water south along the east coast

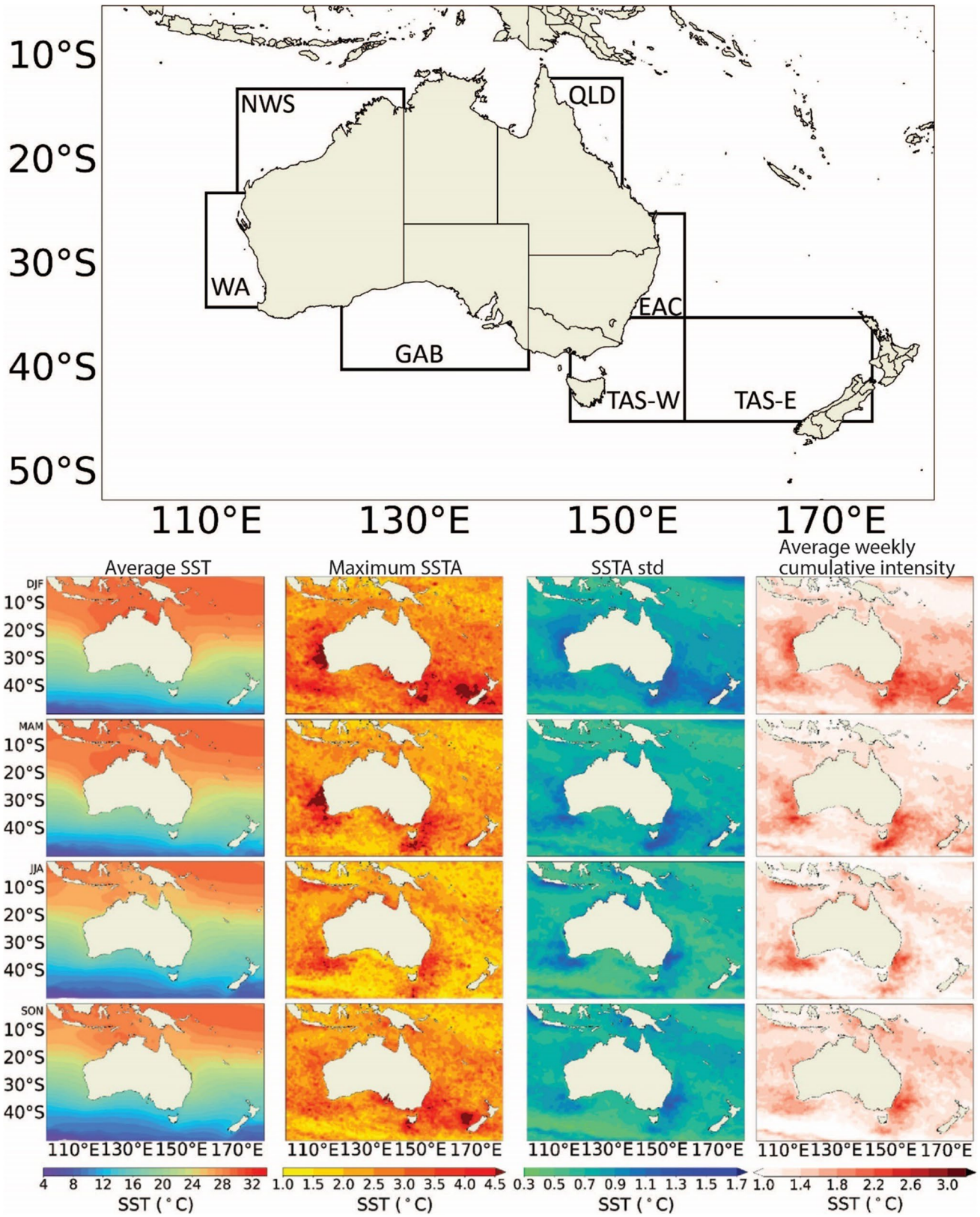

Fig. 2 Ocean temperature statistics for the extended Australian region used in this study separated by season, top row DJF, second row MAM, third row JJA and bottom row SON. These statistics include: average daily SST (first column), the maximum daily SST anomaly (second column), the standard deviation of the daily SST anomalies (third column), and average weekly MHW cumuative intensity (fourth column) for the period 1982–2022

map outlining the key regions mentioned throughout. These include the northwest shelf (NWS), Western Australia (WA), the Great Australian Bight (GAB), Tasman Sea west (TAS-W), Tasman Sea east (TAS-E), the East Australian Current region (EAC) and northeast Queensland (NE QLD). The columns below show a visual representation of average and anomalous daily temperatures categorized by season. Given our focus on the southern hemisphere (SH), we employ austral seasons: summer (DJF), autumn (MAM), winter (JJA), and spring (SON). The first column shows the average daily SST for each season highlighting a consistent trend of higher temperatures in the northern Australian tropical waters, gradually transitioning to cooler temperatures in the southern temperate zones. The second column illustrates the maximum daily SST anomalies, emphasizing regions that frequently experience recurring MHW incidents. Positive ocean temperature anomalies are particularly evident along the Western Australian coast during summer and autumn, aligning with 'Ningaloo Niño;' occurrences (Marshall et al. 2015). The Tasman Sea's eastern and western edges experience substantial SST anomalies during spring and summer. Additionally, the EAC and its extension show strong positive SST anomalies throughout all seasons. The third column shows the standard deviation (std) of daily SST anomalies, closely matching the patterns exhibited in the final column depicting average weekly MHW cumulative intensities per season. On the western coast, elevated std and MHW average intensity are concentrated near the northwest shelf in summer, shifting slightly southward in autumn, and enveloping the southwest coast in winter. The EAC region demonstrates elevated variance and MHW intensities across all seasons, prominently spanning the Tasman Sea, particularly in summer. Notably, during spring, an exceptional maximum SST anomaly is evident in the eastern Tasman Sea. However, the slight divergence between the std and average MHW intensity maps in this instance implies the possibility of a single, disproportionately intense, event compared to the typical spring pattern extreme event.

2.6 Isolating climate drivers through regression analysis

Understanding the individual influence of any single driver is complicated by the fact that they rarely exist in isolation. Figure 3 shows the time series of the ONI, IOD, SAM and STRH from 1982 to 2022 (smoothed using a 20-day running mean), highlighting the difference in the variability of the modes, with the average phase duration of the ONI phases being the longest and those of the STRH the shortest. In Fig. 3 we can also identify periods in which various modes are in phase. For example, in 1997/98 (during the period of strong El Niño) we can see alignment of the positive ONI, positive IOD, negative SAM and positive STRH.

To isolate the impacts of each of the drivers, we used partial regression analysis to remove the signals associated with any other driver with a significant correlation during corresponding seasons (Nicholls 1989; Risbey et al. 2009; Werner et al. 2012; Nuncio and Yuan 2015). To identify correlated drivers, we calculated the correlation coefficient between each of the climate modes using the daily indices, including phases 1–4 of the MJO (phases 5–8 are the inverse of these first four phases). To account for the serial correlation in the time series, we considered the autocorrelation (ρ) to calculate the effective sample size ($n_{eff} = n\frac{1-\rho}{1+\rho}$)(see Marshall et al. 2014) which was used to assess statistical significance using a two-tailed t-test (Student 1908). Table 1 shows the significant correlations between daily driver indices.

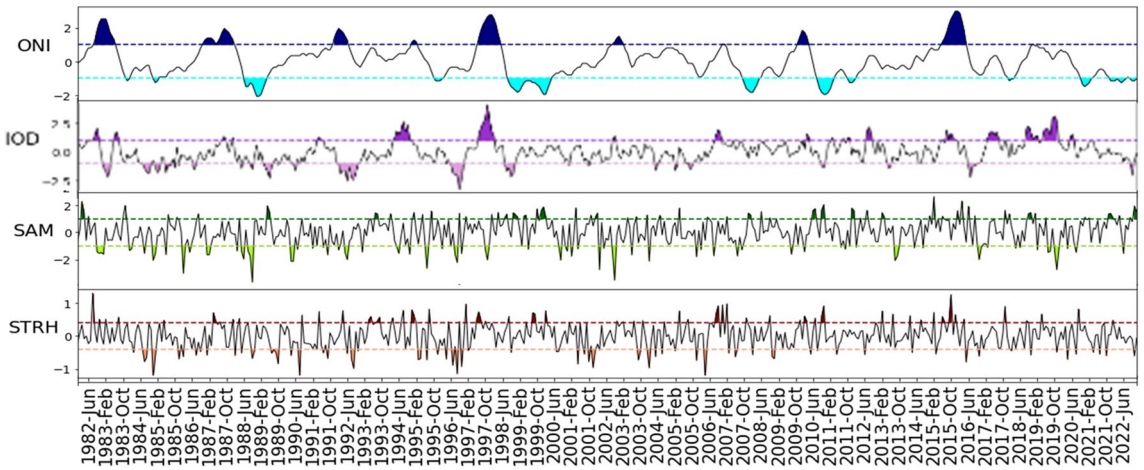

Fig. 3 Timeseries of the Oceanic Niño Index (ONI), Indian Ocean Dipole (IOD), Southern Annular Mode (SAM) and Subtropical Ridge High (STRH) from January 1982 to December 2022, using a 20-day running mean. For each series, dotted lines depict the values used to classify the phases of each index. Shading highlights instances when the index surpasses these levels, indicating positive or negative phases

To remove the signal of any driver, we first used partial correlation analysis to identify the part of the SST anomaly that is explained by a climate driver. This signal is then removed from the original dataset to create a new set of daily SST anomalies used to make composite maps during the relevant positive and negative phases. While this method attempts to completely remove the signal of a driver, it is important to note some of the influence may remain, particularly if there are lagged impacts. To each of these maps, we also include MSLP and wind speed anomalies, where relevant, to assess the mechanisms that could lead to the accumulation of heat in any region.

2.7 Understanding the mechanisms driving extreme regional ocean warming

Lastly, our analysis looks at understanding the compounding influences of ENSO and the MJO. The sources of excess heat in the Ocean's upper layer can be evaluated using the heat budget equation (Eq. 1). We use this heat budget equation to better understand the mechanisms that drive ocean warming in the WA region (see Fig. 2) during La Niña states with the various phases of the MJO, following the methodology of Marshall and Hendon (2014).

$$\frac{\partial T}{\partial t} = \frac{Q_{net}}{\rho C_p H} - \left[u\frac{\partial T}{\partial x} + v\frac{\partial T}{\partial y}\right] - w\frac{\partial T}{\partial z} + res \tag{1}$$

where the temperature tendency ($\frac{\partial T}{\partial t}$) is due to contributions from the total heat flux (Q_{net}) (scaled by the density of seawater ($\rho = 1025$ kg/m^3), the heat capacity of water ($C_p = 3850$ J/kgC) and the daily varying mixed layer depth (H)), the horizontal advection $\left(u\frac{\partial T}{\partial x} + v\frac{\partial T}{\partial y}\right)$, and the vertical advection ($w\frac{\partial T}{\partial z}$), where $u\frac{\partial T}{\partial x}$, $v\frac{\partial T}{\partial y}$ and $w\frac{\partial T}{\partial z}$ represent the current speeds, depth-averaged over the mixed layer depth, multiplied by the temperature gradients in the zonal, meridional and vertical directions respectively. There is also a residual term which approximates smaller contributions from entrainment and diffusion and second order terms.

We also consider the combined influence of La Niña with the MJO in the NE QLD region (see Fig. 2). As this region is directly impacted by changes to tropical wind patterns, we investigate the role of Ekman transport, also following the methodology of Marshall and Hendon (2014), by considering the proportion of total horizontal convergence ($\frac{\partial u}{\partial x} + \frac{\partial v}{\partial y}$) (calculated from the anomalous geostrophic meridional and zonal surface currents) that is due to Ekman convergence ($\frac{\partial u_E}{\partial x} + \frac{\partial v_E}{\partial y}$) (Talley et al. 2011). Here, the Ekman convergence is directly related to the Ekman currents arising from anomalous meridional (τ_y) and zonal (τ_x) wind stress using Eqs. 2 and 3.

$$v_E = -\frac{1}{f\rho}\frac{\partial \tau_x}{\partial z} \tag{2}$$

$$u_E = \frac{1}{f\rho}\frac{\partial \tau_y}{\partial z} \tag{3}$$

Table 1 Correlation coefficients between daily climate driver indices, including the phases of the MJO

Summer (DJF)	Niño34	IOD	SAM	STRH	Phase1	Phase2	Phase3	Phase4
Niño34	1					0.061	0.061	0.032
IOD		1			**-0.12**	**-0.11**	-0.049	0.038
SAM	**-0.19**	-0.083	1		-0.077	**-0.14**	**-0.12**	-0.043
STRH	0.078	-0.033	0.069	1		**0.11**	**0.13**	**0.097**
Autumn (MAM)	Niño34	IOD	SAM	STRH	Phase1	Phase2	Phase3	Phase4
Niño34	1				0.073	**0.12**	0.096	
IOD	-0.04	1			0.044		-0.04	-0.057
SAM			1		-0.05			0.045
STRH		0.054	0.042	1		**0.15**	**0.19**	**0.11**
Winter (JJA)	Niño34	IOD	SAM	STRH	Phase1	Phase2	Phase3	Phase4
Niño34	1							
IOD	**0.3**	1				0.078	**0.1**	0.05
SAM		0.066	1			0.057	**0.1**	0.074
STRH	0.074	**0.15**	**0.12**	1	**0.3**	**0.32**	**0.18**	**-0.12**
Spring (SON)	Niño34	IOD	SAM	STRH	Phase1	Phase2	Phase3	Phase4
Niño34	1				**0.18**	**0.28**	**0.22**	
IOD	**0.45**	1			**0.18**	**0.14**		**-0.13**
SAM	**-0.13**	**-0.12**	1		-0.083	-0.066		0.059
STRH	0.07	-0.11	0.077	1	**0.15**	**0.25**	**0.22**	0.033

Those with p-values < 0.05 are shown in bold, those with p-values > 0.1 are not shown

3 Results

3.1 Average seasonal states with each driver

3.1.1 ENSO

The average daily atmospheric and oceanic states during the phases of ENSO are shown in Fig. 4. ENSO is strongly correlated to the IOD in winter and spring (Table 1). However, this correlation is significant with the IOD lagged from -3 to + 6 months (Werner et al. 2012), and so we have removed the IOD signal from the entire time series. The influence of SAM has also been removed during austral spring and summer. The phases of ENSO have a strong seasonal cycle, with event build-up in the late winter and spring months, peak during summer, and decline through autumn (Philander 1983). The composite maps for El Niño (Fig. 4) show general cooling in the northeast during all seasons, and cooling along the west coast during summer and autumn as well as in the eastern Tasman Sea during summer, autumn and winter. In autumn, as the El Niño event is declining, there is evidence of warming in the northwest region and along the east coast.

The composite maps for La Niña states show broader regions of anomalous warming. During spring, as La Niña is building up, we see positive SST anomalies in the NE QLD and NWS regions and starting to develop on the west coast. During austral summer and autumn, in the following year, the positive SST anomalies show the strong signal associated with 'Ningaloo Niño,' which persists into the winter. There is also a strong warming signal in the Tasman Sea during autumn and winter. The wind patterns show stronger northeasterlies during La Niña in the northeast region in all seasons (Fig. 4, second column). During austral spring, these winds bring warm water onshore and contribute to the warming through promotion of downwelling (Fig. 4b). However, during summer and autumn, these winds divert further east from the Australian mainland and the heating signal remains offshore.

The MHW hazard index values associated with El Niño or La Niña phases in each season can be seen in Fig. 5. The higher hazard rating during La Niña closely matches the SST anomaly maps in Fig. 4. There is a very high MHW hazard rating in spring and winter in the northeast region, and higher than average during summer. The hazard rating in the WA region builds up during summer and reaches an extreme rating during autumn before starting to decline again in winter.

During El Niño, we can see a lower-than-average MHW hazard rating in the northeast region during spring and winter and a lower-than-average to very low hazard rating along the west coast during summer and autumn. During autumn (Fig. 5e), we also see regions of very high MHW hazard in the northwest of Australia, particularly around the Indonesian island of Java, as well as stretching across the Tasman Sea. As there isn't a corresponding SST warming signal in the Tasman Sea (Fig. 4e), it is likely that these MHWs are due to other drivers, as the influence of these was not removed from the MHW hazard level analysis.

3.1.2 IOD

The IOD significantly impacts oceanic and atmospheric patterns, influencing Australian climate most noticeably from May through to November, with December to April dominated by the Australian monsoon (Saji et al. 1999). The ENSO signal was removed from the entire timeseries for the IOD analysis, as well as the influences of SAM during spring and the STRH during winter.

Changes to atmospheric circulation during the phases of the IOD are shown in Fig. 6. During austral winter and spring seasons, enhanced westerlies draw warm waters to the northwest coast during the negative phase (Fig. 6b, h). Conversely, enhanced westerlies during the positive phase have the opposite effect (Fig. 6a, g). During the summer season, although we also see the accumulation of heat in the ocean surface on the northwest coast (Fig. 6d), the wind patterns are not consistent with those associated with the IOD as they are dominated by the Australian monsoon during these months. The same can be seen during autumn (MAM), however to a lesser extent, as these months are impacted by a combination of the IOD and the Australian monsoon.

The impacts on the SST anomalies are most apparent in the northwest region, with positive SST anomalies during the negative IOD phase and negative SST anomalies during the positive phase in all seasons. However, the MHW hazard maps shows that the increased risk only reaches the coastline in this region during winter (Fig. 7h). There is also region of high hazard on the northeast coast during spring (Fig. 7b), which may be due to the likelihood of La Niña co-occurring with negative IOD events, with the reverse shown during the positive phase (Fig. 7a). The very low hazard region in the western Tasman Sea during spring is more likely due cooling experienced in the Tasman Sea during the negative phase of SAM (Fig. 8b), which is statistically significantly correlated with the positive IOD in spring (Table 1).

3.1.3 SAM

Composite maps of atmospheric and oceanic anomalies during the phases of SAM are shown in Fig. 8, with the signals of ENSO during spring and summer, the IOD during spring, and the STRH during winter removed.

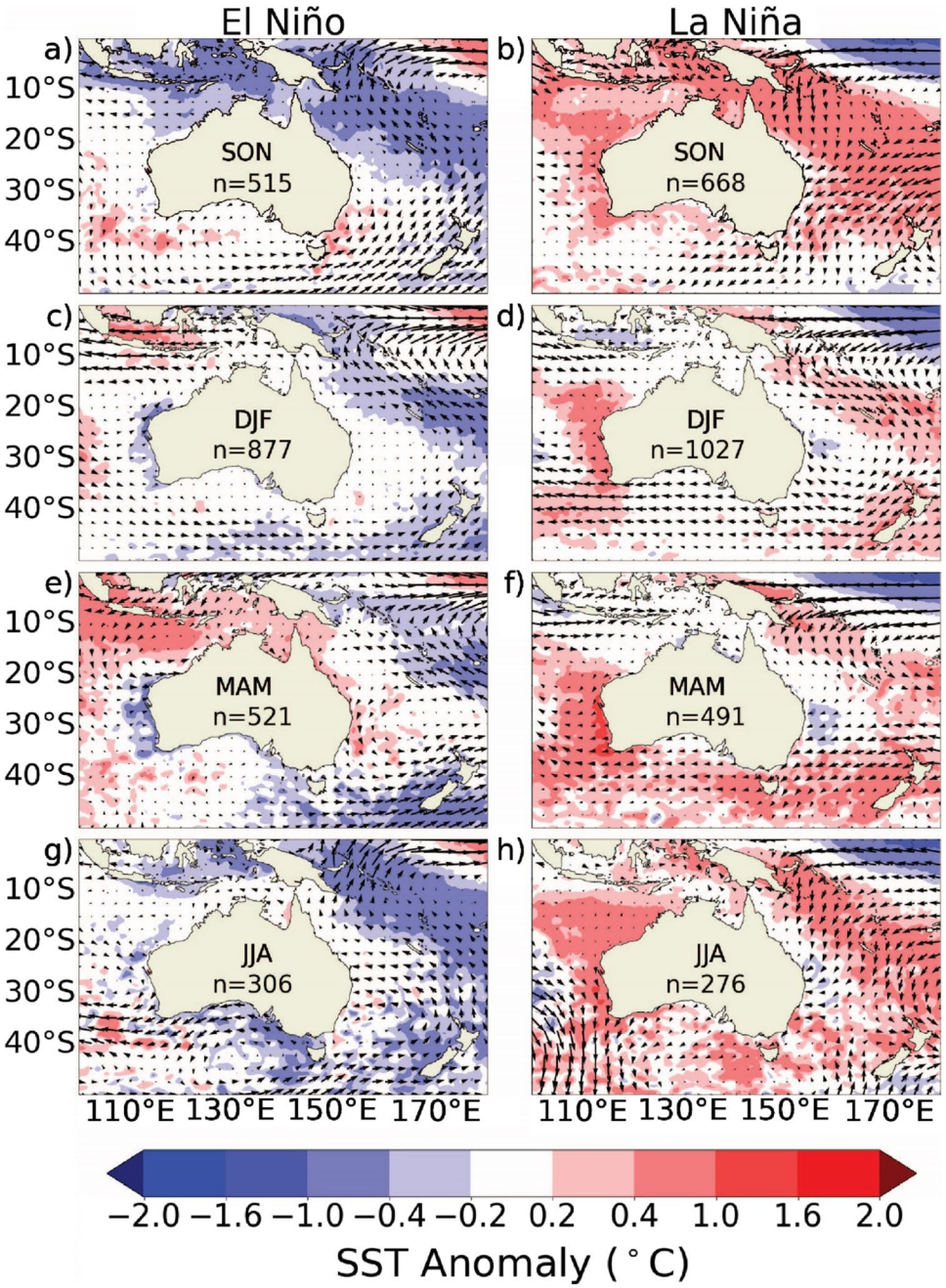

Fig. 4 The maps show the average daily anomalous atmospheric and oceanic conditions during El Niño (left column) and La Niña (right column) events, from 1982–2022. These maps are separated by season, spring (SON) (**a**-**b**), summer (DJF) (**c**-**d**), autumn (MAM) (**e**-**f**) and winter (JJA) (**g**-**h**). Shading depicts the SST anomalies, contours represent the MSLP anomalies and quiver bars show anomalous wind patterns. The sample size (n) shows the number of days in the period used to create each of the composite maps

From the number of days (n) of each phase, we can see that the positive SAM is more likely during austral spring, while the negative SAM occurs more often during winter. The most obvious pattern of SST anomalies during the positive phase of SAM is the heating signal evident across the Tasman Sea in spring, summer, and autumn. Conversely there is noticeable cooling in the same region during the negative phase in summer and spring.

During the positive phase of SAM, there are several regions with a positive MHW hazard rating. The Tasman Sea shows a very high MHW hazard rating during summer, autumn and winter, and the northeast shows a very high hazard rating during spring and summer. However, this pattern seems to closely resemble the warming pattern associated with La Niña during those times (Fig. 4b, d). Despite strong anomalous cooling in the Tasman Sea during the negative phase of SAM in spring and summer (Fig. 8b, d), the MHW hazard level rating does not show any significant reduction during these periods (Fig. 9b, d).

3.1.4 STRH

The influences of the SAM and IOD in winter were first removed as they are significantly correlated to the STRH

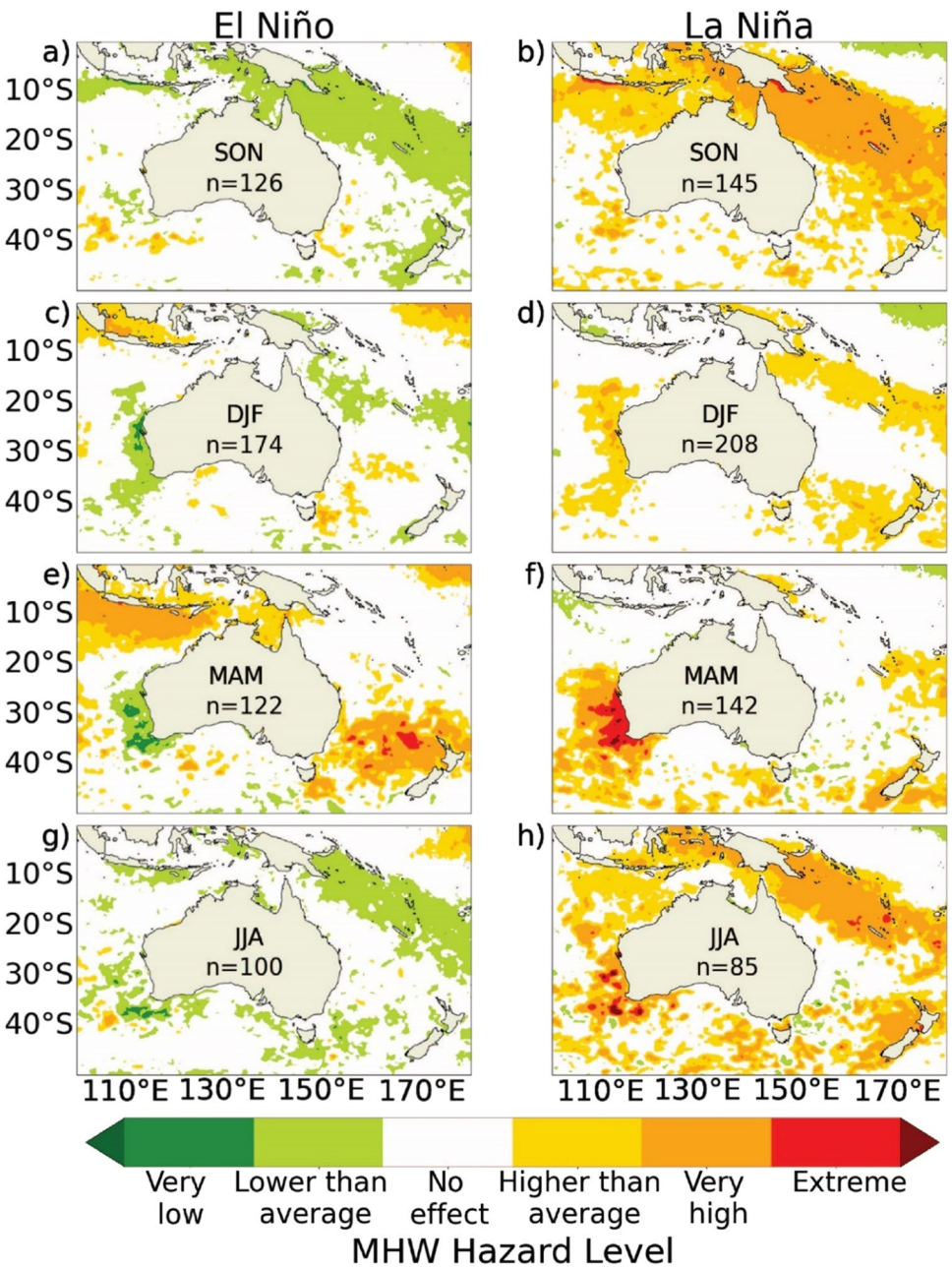

Fig. 5 MHW hazard rating for El Niño (left column) and La Niña (right column) phases, separated by season, spring (SON) (**a**-**b**), summer (DJF) (**c**-**d**), autumn (MAM) (**e**-**f**) and winter (JJA) (**g**-**h**). The hazard index reflects the average excess temperature due to MHWs (°C) for the phase and season of interest. When the value is < -1.5°C, we say the MHW hazard level is very low. When the value is between -0.5°C and -1.5°C, it is seen as lower than average. When it is between -0.5°C and 0.5°C, we consider there is no effect. When it is between 0.5°C and 1.5°C, it is seen as higher than average. When between 1.5°C and 2.5°C, it is seen as very high. And finally, when it is > 2.5°C, we classify it as extreme

index during this season (Table 1). The atmospheric patterns are the most distinctive compared to the other drivers (Fig. 10). The positive STRH phase shows the high pressure, anti-cyclonic system centred over the Tasman Sea, with corresponding winds moving in an anti-clockwise direction. These high-pressure systems are associated with clearer skies and increasing descending warm air, contributing to extra heating in the TAS-E and in the GAB (Fig. 2 for locations) during spring and summer. The wind vectors also show strong winds moving warm air from the Australian continent south into the region of the GAB, contributing to the extra warming in this region.

During spring and summer, we can also see a heating signal off the NWS, and in an extended region of WA during summer. However, the wind patterns during these phases do not explain this phenomenon. From Table 1, we see that there is a strong and significant correlation between the STRH and the MJO in phases 2, 3 and 4 during summer. These phases are associated with warmer than usual SSTs in this northwest region (Fig. 12) and, could be the cause of these anomalies.

The opposite anomalous atmospheric pattern is apparent during the negative phase of the STRH (Fig. 10). Here, we can see low-pressure, cyclonic systems centred over the

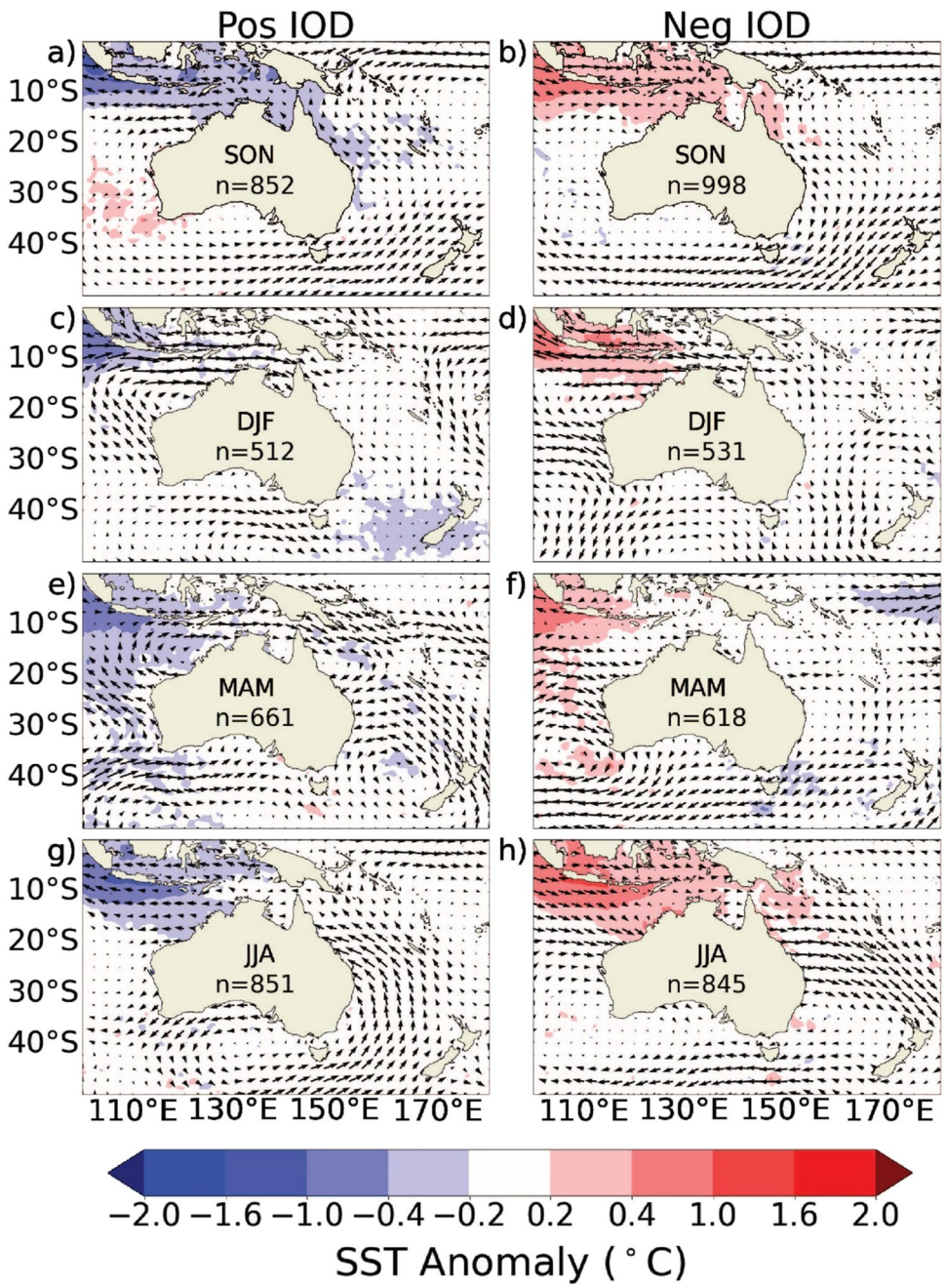

Fig. 6 As in Fig. 4 but for the IOD

Tasman Sea, along with strong anomalous winds moving in a clockwise direction around these low-pressure cells. We can see signals of warming in the NE QLD region during spring, summer, and autumn as warm, dry air is being transported north from the centre of the Australian continent into this region.

Despite the consistency of these warming patterns, the MHW uniformity of the hazard ratings for this driver are low in most seasons (Fig. 11). Summer shows the strongest influence, with a higher than average to very high hazard off the northeast coast during the negative phase (Fig. 11d), and a lower-than-average MHW hazard during the positive phase (Fig. 11c). The low sample size for the weekly samples compared to the daily sample sizes in Fig. 10 suggests that these STRH phases are short lived and restrict their ability to contribute to sustained warmer ocean temperatures, i.e., MHWs.

3.1.5 MJO

The MJO is significantly correlated to the STRH in both spring and summer, and with Niño34 index during spring (Table 1), and so the influences of these have been removed. The MJO is distinctive from the drivers we have considered above, as its eight phases are defined by the region of the centre

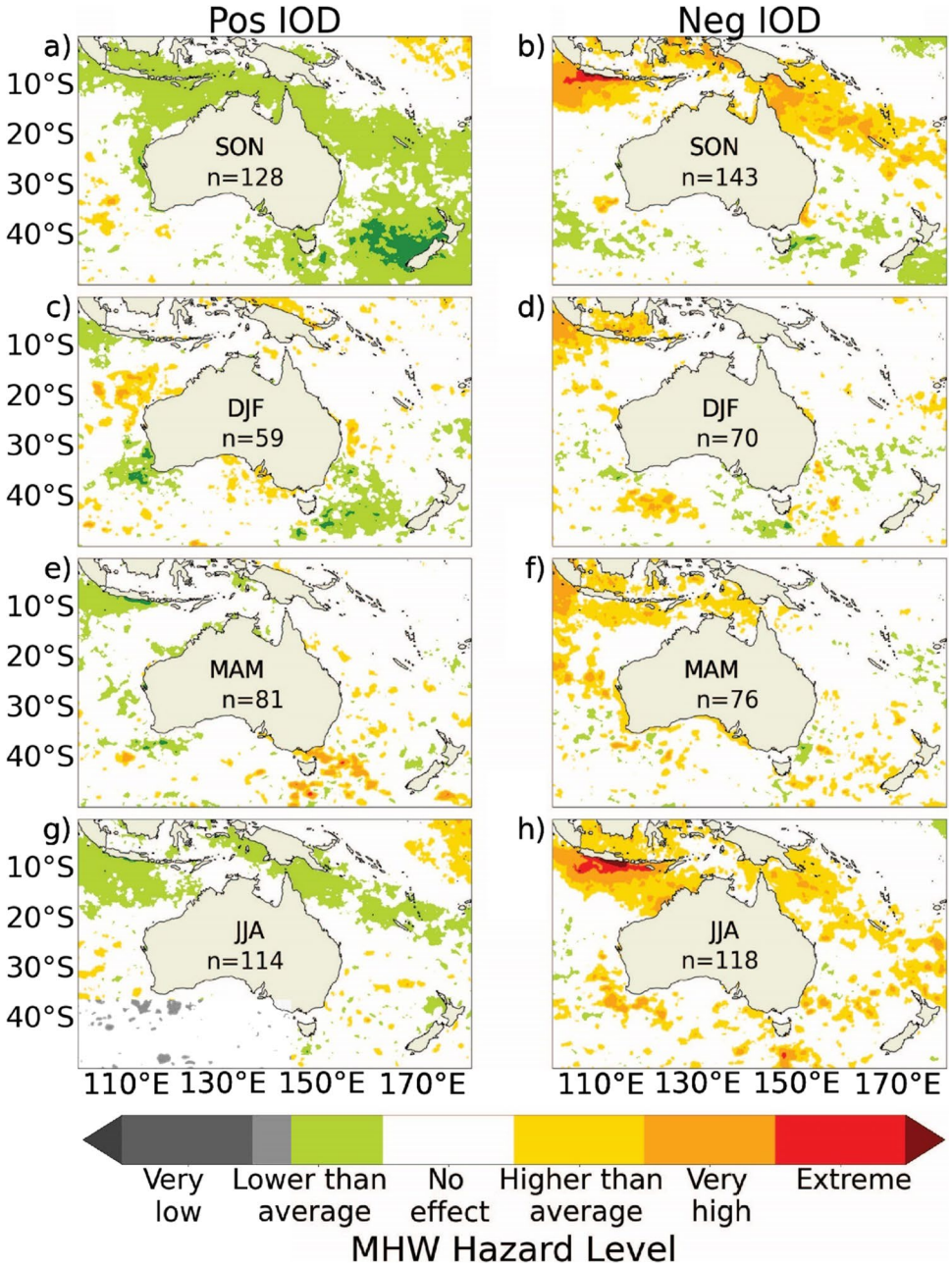

Fig. 7 As in Fig. 5 but for the IOD

of convection of the eastward propagating storm system. To simplify this analysis, we have grouped the phases in pairs and restricted our analysis to the austral spring (SON) and summer (DJF) months when the MJO's convective centre shifts to the south of the equator and has the greatest impacts on the Australian region (Zangvil 1975; Wheeler and Hendon 2004).

The strongest warming signal is seen on the NWS in summer during MJO phases two and three. Marshall and Hendon (2014) found this to be attributed to vertical advection, due to Ekman transport in response to the strengthened easterly winds. Heating off the northeast coast can be seen in response to extremely low wind speeds in phases four and five during spring, and in summer during phases six and seven, although the anomalously low winds is less striking.

Interestingly, in spring during phases six and seven, a low-pressure system over the Tasman Sea can be seen to contribute to warming off the northeast region (Fig. 12e), by pushing warm, continental air into the region in much the same way as the STRH, with the opposite seen in phases two and three, despite our removal of the STRH signal.

During the summer months in phases six and seven, there is also a strong heating signal in the Tasman Sea. This region is especially interesting as it is the strongest signal shown in our MHW hazard analysis (Fig. 13f).

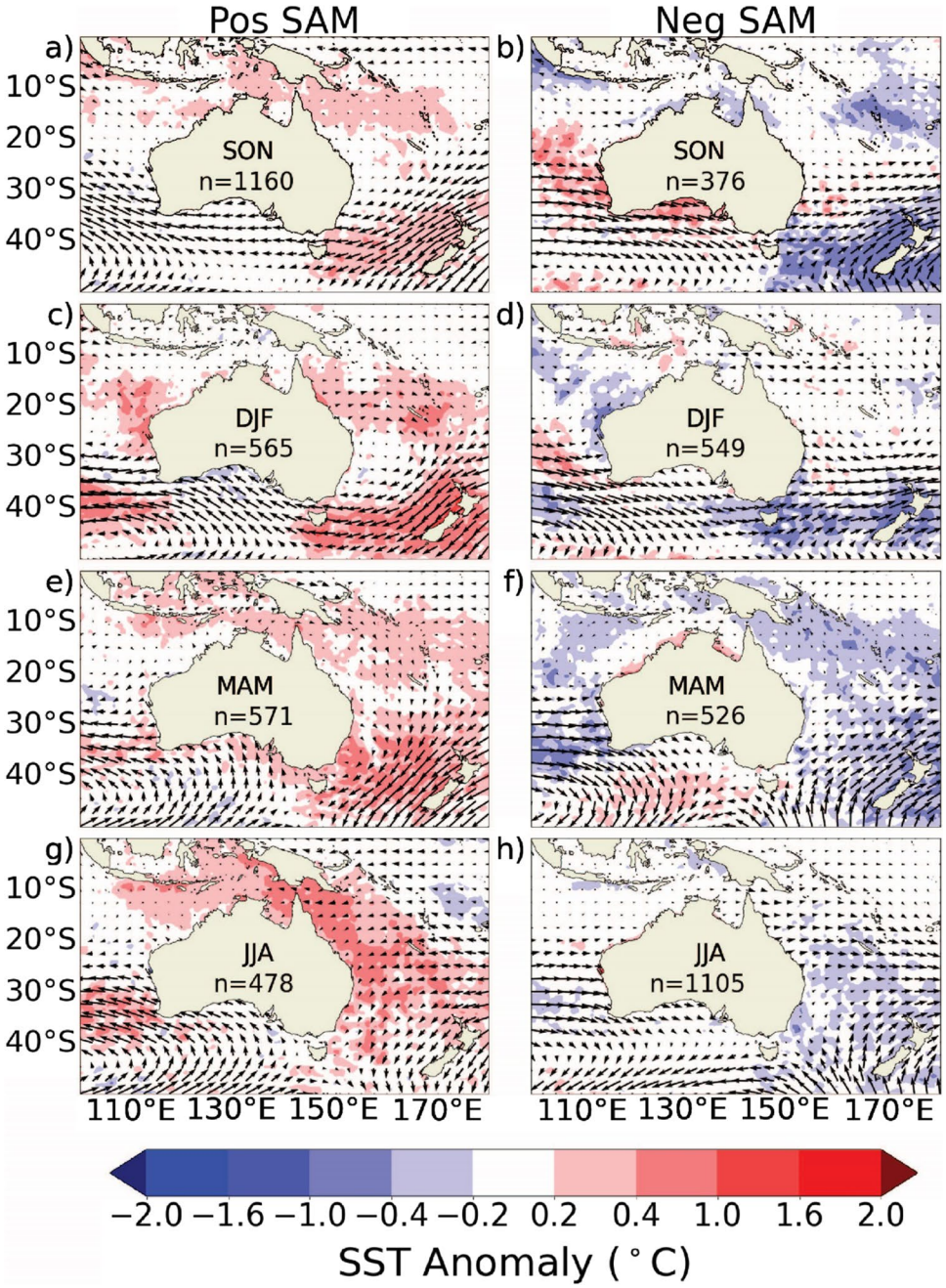

Fig. 8 As in Fig. 4 but for the SAM

3.2 Leading driver of SST variability at each location

From our analysis so far, we can see that there are several regions influenced by multiple drivers. To qualitatively show the drivers of most importance, we have calculated the simultaneous, daily correlation between each of the driver indices and positive SST anomalies at each grid point.

Figure 14 shows the driver with the highest correlation with positive SST anomalies based on daily values (left column) and the corresponding correlation coefficient between the index of the leading driver and SST anomalies (right column). Autocorrelation is accounted for using a reduced effective degrees of freedom in the statistical significance test (Marshall et al. 2014). The prevalence of La Niña is evident, indicating its dominance in driving positive SST anomalies in the NE QLD and WA regions for all seasons. The influence of La Niña on ocean warming endures in these regions for up to four weeks (Supplementary Figs. 1–4). El Niño emerges as the strongest simultaneous driver in the NWS and the NE QLD regions during autumn and winter (Fig. 14e, g) becoming increasingly dominant in the NWS during summer and autumn with a one to four week lag (Supplementary Figs. 1–4).

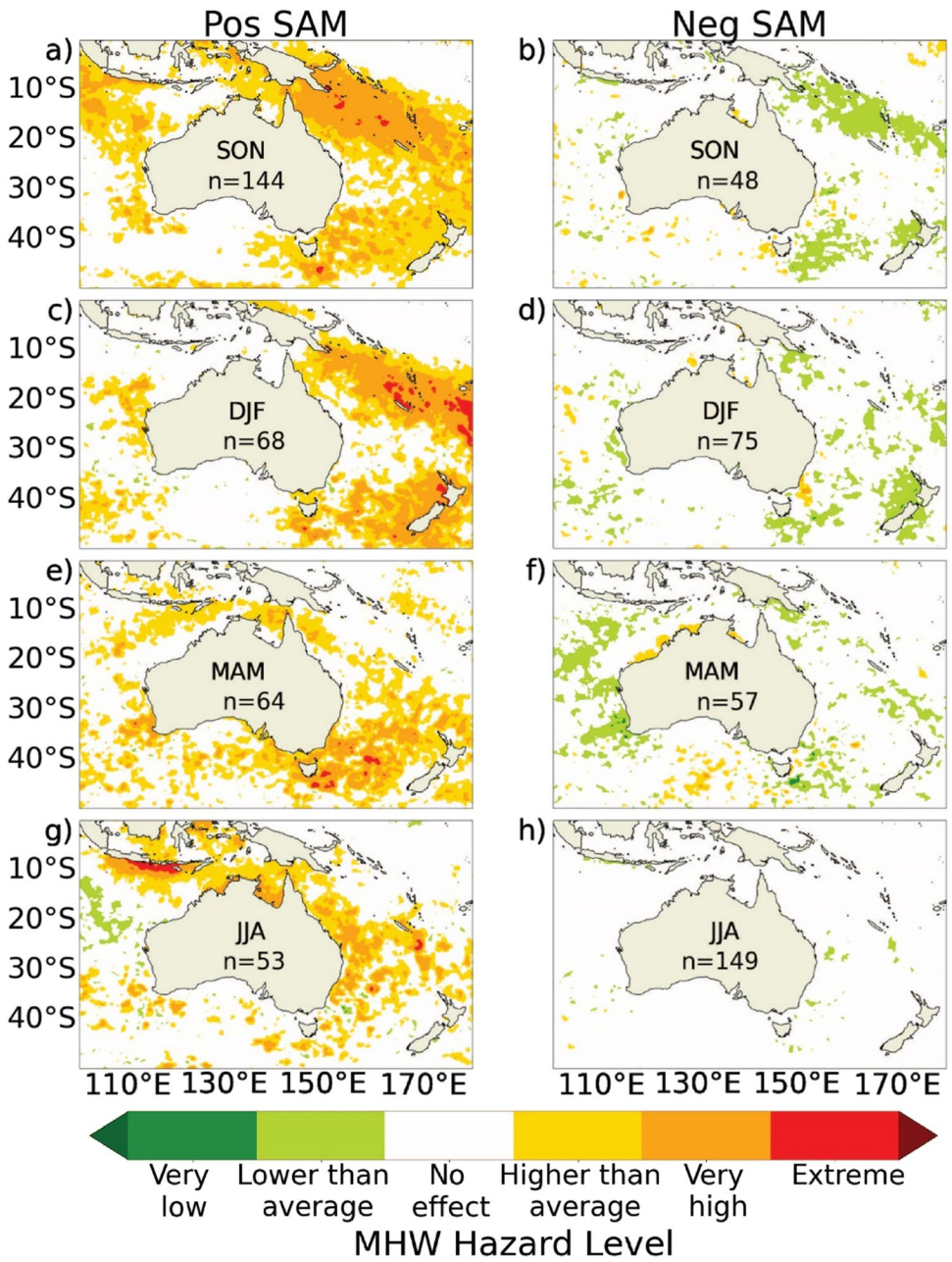

Fig. 9 As in Fig. 5 but for the SAM

During the summer months, we observe the highest number of individual leading drivers, with most drivers being present (Fig. 14c). While La Niña is dominant over a smaller proportion of the domain in summer compared to spring, it still influences the NE QLD, WA, and TAS-E regions. Our previous analysis suggests that La Niña has the highest correlation value in summer in the TAS-E and TAS-W regions due to its connection with the positive phase of the SAM, which has been associated with significant SST heating and MHWs in the Tasman Sea during spring and summer.

The negative phase of the STRH emerges as the dominant driver in the NE QLD region during summer (Fig. 14c), continuing into autumn and winter, and the positive phase of the STRH is shown to be the strongest influence of positive SST anomalies in the GAB. However, the influence of the STRH lessens considerably after a week (Supplementary Fig. 1), with almost no significant correlation after two weeks (Supplementary Fig. 2). The positive phase of the IOD does not appear to correspond with positive anomalies in any region, while the negative IOD dominates the NWS domain and remains the strongest driver in the spring and winter months up to four weeks later (Supplementary Fig. 4). The MJO is only a primary influence when in phase 3

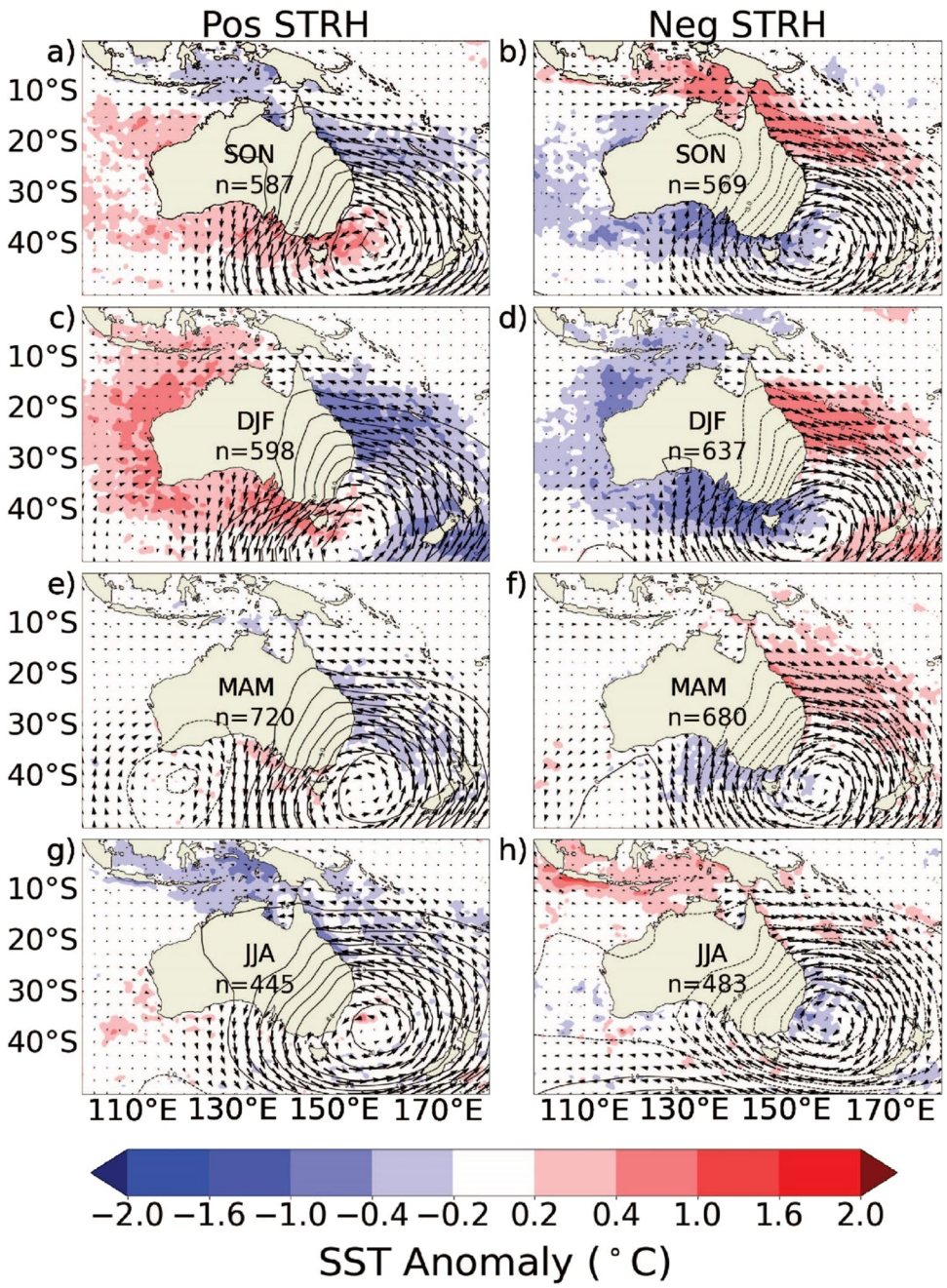

Fig. 10 As in Fig. 4 but for the STRH

(other phases not shown), where it is the leading driver during summer in the NWS (Fig. 14c). The influence of the MJO also decreases after two weeks (Supplementary Fig. 2), however it remerges as the stronger driver in the GBR region in winter with a one to four week lag (Supplementary Figs. 1–4).

It is also important to note that there are regions that are not significantly correlated to any driver on this simultaneous, daily timescale. The EAC region, for example, does not show any statistically significant correlations in any season and the GAB is blank during autumn and winter.

3.3 Compound drivers: modulation of ENSO influences by the MJO

Building on our earlier evaluation of individual drivers, we now shift our focus towards understanding how multiple drivers work together to influence SST distributions. For this analysis, we examine how the MJO can alter the influence of La Niña events in two different regions during summer (DJF). In Fig. 15, the left column shows composites of SST and wind anomalies corresponding to each of the phases of the MJO. The middle column shows the phases of the MJO during La Niña periods. The right

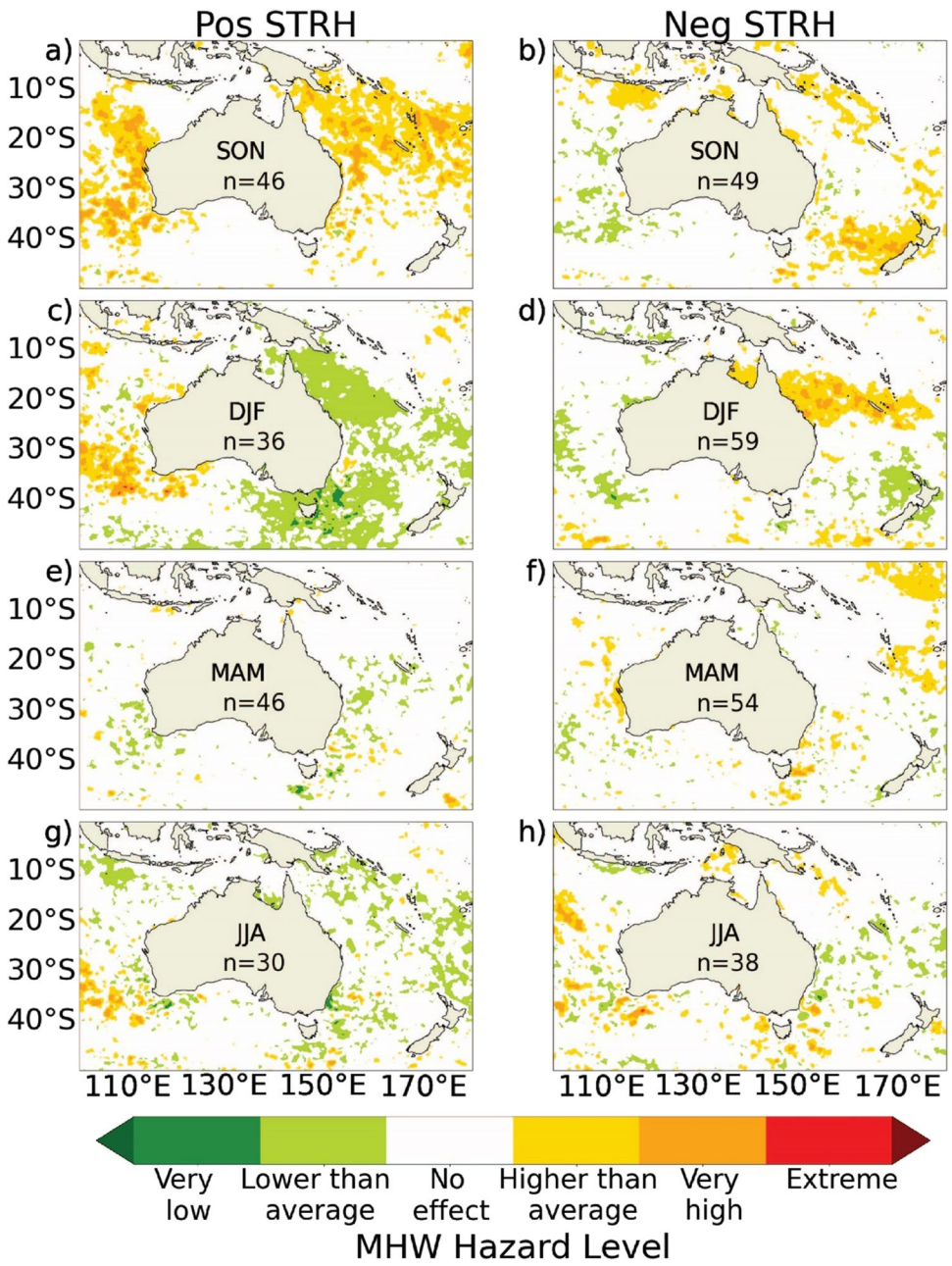

Fig. 11 As in Fig. 5 but for the STRH

column shows these same composites with the average summer La Niña conditions (Fig. 4d) removed to represent the explicit influence of the MJO. The La Niña state is the leading driver of positive SST anomalies in the WA region (Fig. 4), but we can see from both the middle and right columns that the MJO can influence this signal, with stronger anomalies evident in phases 5–6 and weaker anomalies in phases 1, 2 and 8. We have seen from our previous analysis that SSTs to the northeast of Australia are generally positive during La Niña in all seasons (Fig. 4), and remaining offshore during summer. In the middle column of Fig. 15, we can see this warming coming onshore during MJO phases 5–8, with the MJO contributing to this warming. Finally, we can see a warming pattern in the Tasman Sea during MJO phases 2, 5, 7–8, which could be due to a high pressure system in the region caused by an atmospheric Rossby wave train driven by the propagation of the MJO as shown in Wang and Hendon (2020) and Marshall et al. (2023).

Both ENSO and the MJO alter tropical wind patterns, with the easterly trade winds strengthened during La Niña and tropical winds converging towards the convective centre of the MJO, where the location is dependent on the phase of the MJO. In the left column (Fig. 15), MJO phases 1–3 show strengthened easterlies, and phases 4–5 show winds converging over Australia, causing stronger easterlies in the east and

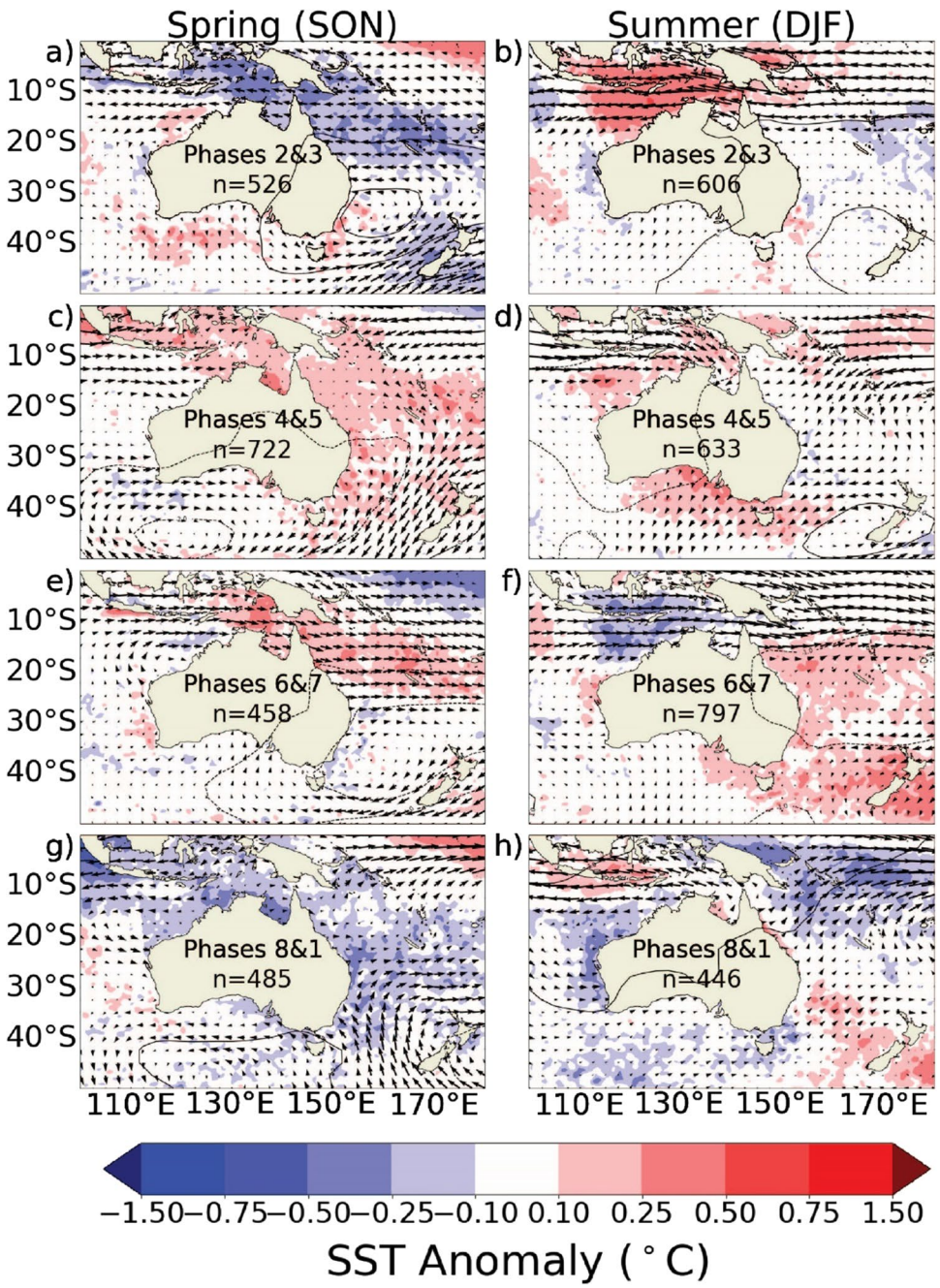

Fig. 12 As in Fig. 4 but for the phase pairs of the MJO

stronger westerlies in the west. During MJO phases 6–7, the direction changes to stronger westerlies, and finally in phase 8 the winds divert from Australia causing stronger westerlies in the east and stronger easterlies in the west.

To better understand the mechanisms that drive an increase to the warming signal associated with La Niña in the Western Australia region during phases 4–6 of the MJO and a decrease in this warming signal during phases 8–1-2, we performed a heat budget analysis (Eq. 1) in the WA box region 110°-116°E, 21°-34°S (Fig. 2).

We calculated the average contributions of each of the components of the heat budget equation corresponding to the phases of the MJO during La Niña periods in summer and removed the average of all La Niña summer events. The results are shown in Fig. 16a, with the *x*-axis showing the MJO phase and the coloured lines representing the composites of different components of the heat budget.

The temperature within the mixed layer in this region increases sharply in phases 4–5 before dropping and reaching a minimum in phase 8. During the positive temperature change (phases 4–5), positive heat fluxes and vertical

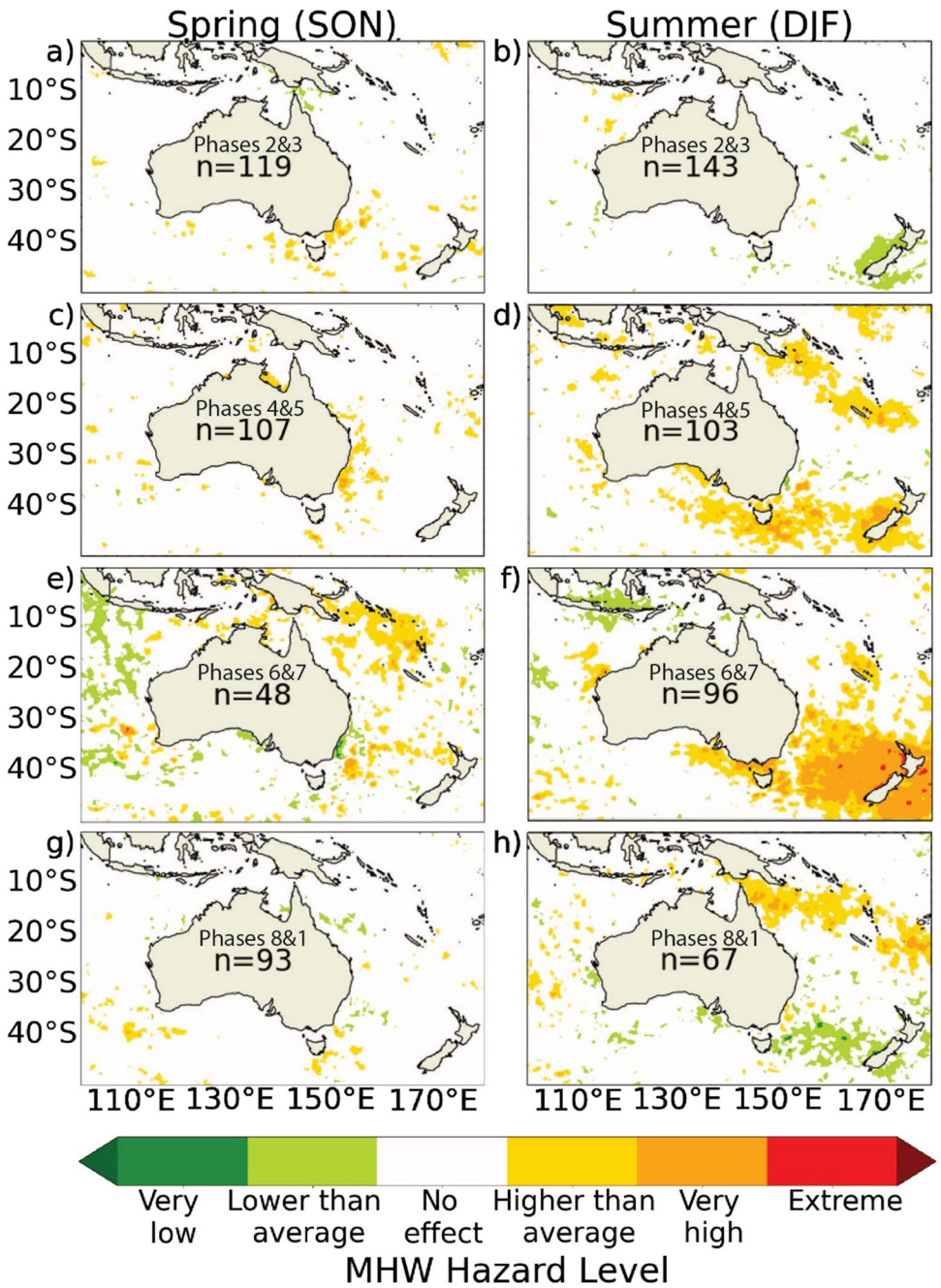

Fig. 13 As in Fig. 5 but for the phase pairs of the MJO

advection play prominent roles, whereas the negative temperature change (phase 6–8) is primarily governed by the vertical advection term. This vertical advection is likely linked to an increase in upwelling driven by wind changes induced by the propagation of the MJO. Phases 4–5 are characterized by westerly winds in the northwest region, with the winds shifting southward along the west coast in phase 5. These wind patterns contribute to the positive vertical advection observed in these phases (Fig. 16a), primarily driven by downwelling processes. Conversely, the wind direction shifts in phases 8–1, where strong southerly winds lead to a decrease in vertical advection through enhanced upwelling.

It is noteworthy that even after isolating each MJO phase and accounting for the average La Niña summer imprint, a positive horizontal advection contribution persists across all phases, primarily associated with the intensification of the Leeuwin Current during La Niña periods (Feng et al. 2003).

In our analysis of ENSO, we have observed a consistent pattern of warming in the NE QLD region during La Niña (refer to Fig. 4), though typically, these warmer waters do not reach inshore. However, during MJO phases 6–8, we

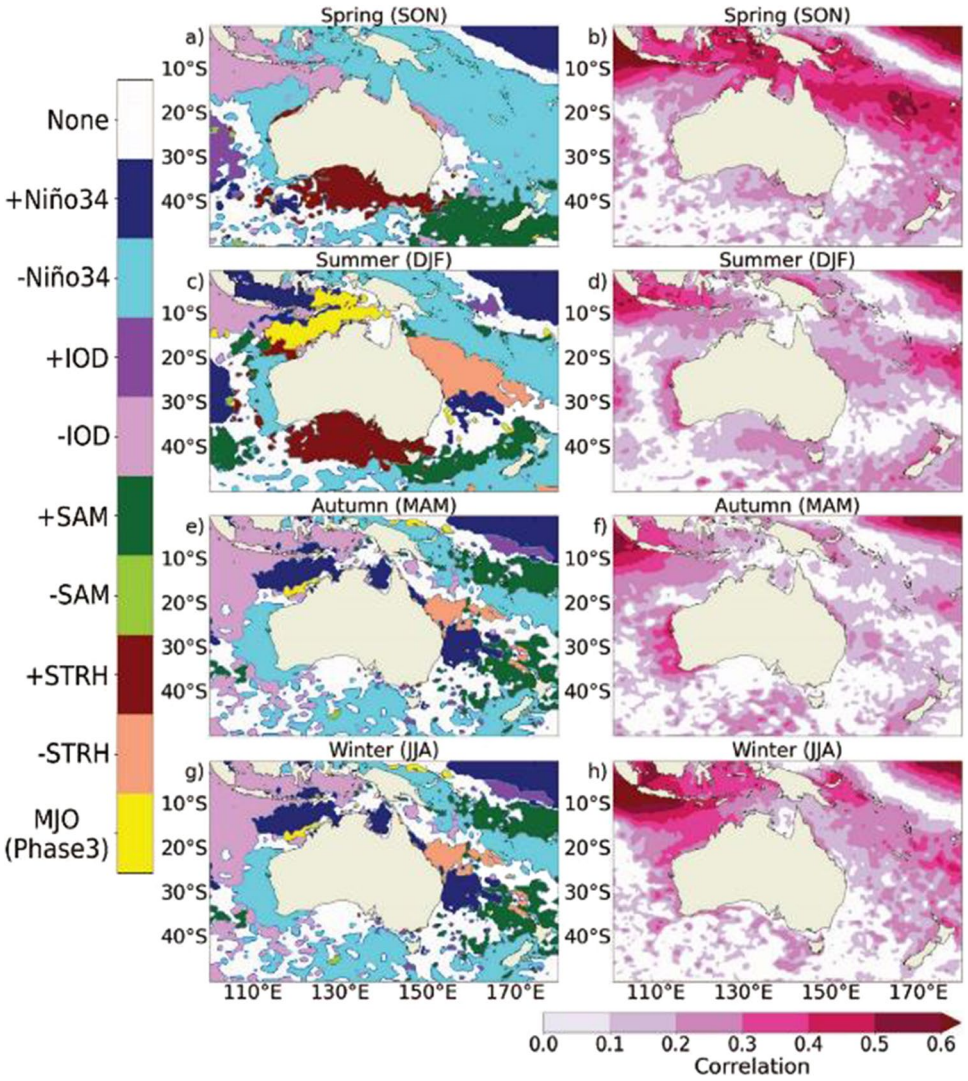

Fig. 14 The left column shows the driver with the highest correlation to positive SST anomalies with the right column showing the respective correlation between the index of the leading driver and SST anomalies. Following the previous analysis, these maps are separated by season, spring (SON) (**a**-**b**), summer (DJF) (**c**-**d**), autumn (MAM) (**e**-**f**) and winter (JJA) (**g**-**h**) Only analysed drivers with a statistically significant correlation ($p < 0.05$) are shown

have detected a distinct warming signal in this region (see Fig. 15, third column). Considering the substantial impact of the MJO on tropical climate through its modulation of wind patterns, we also investigated the role of Ekman transport of this warmer water towards inshore NE QLD (142°-150°E, 12°-24°S; Fig. 2).

The average Ekman convergence and total convergence was calculated during each phase of the MJO during La Niña (Eqs. 2 and 3), with the average summer La Niña values (Fig. 4d) removed, as in the right column in Fig. 15.

The results in Fig. 16b show the average Ekman convergence and total convergence with phases of the MJO. The convergence is negative in MJO phases 1–3, positive in phase 4 before reaching its maximum in phase 5, remains positive in phase 6, and falls below zero again in phases 7–8 (Fig. 16b). The signal of the convergence shows a one MJO phase lag to the winds, which have their maximum westerly strength in MJO phases 3–4. The SST expression is lagged two phases to the convergence due to the thermal inertia of the ocean, with the positive SST anomalies shown in MJO phases 6–8 (Fig. 15).

These results provide evidence affirming the influence of the MJO in modulating the effects of La Niña on ocean temperatures surrounding Australia during the summer season. The profound shifts in wind patterns associated with MJO phases underpin this relationship. While extreme heat is typically expected in the Western Australian region during the summer months of La Niña periods, by incorporating our understanding of the added influence of the MJO we gain a clearer view of the sub-seasonal outlook. Moreover, in the Queensland context, this insight shows the mechanisms through which the MJO, in conjunction with La Niña, triggers warming by facilitating the onshore movement of anomalously warm waters, present during La Niña periods, via Ekman transport. This represents a significant advancement in understanding the complex dynamics of these climate drivers and their cascading influences on ocean temperature extremes.

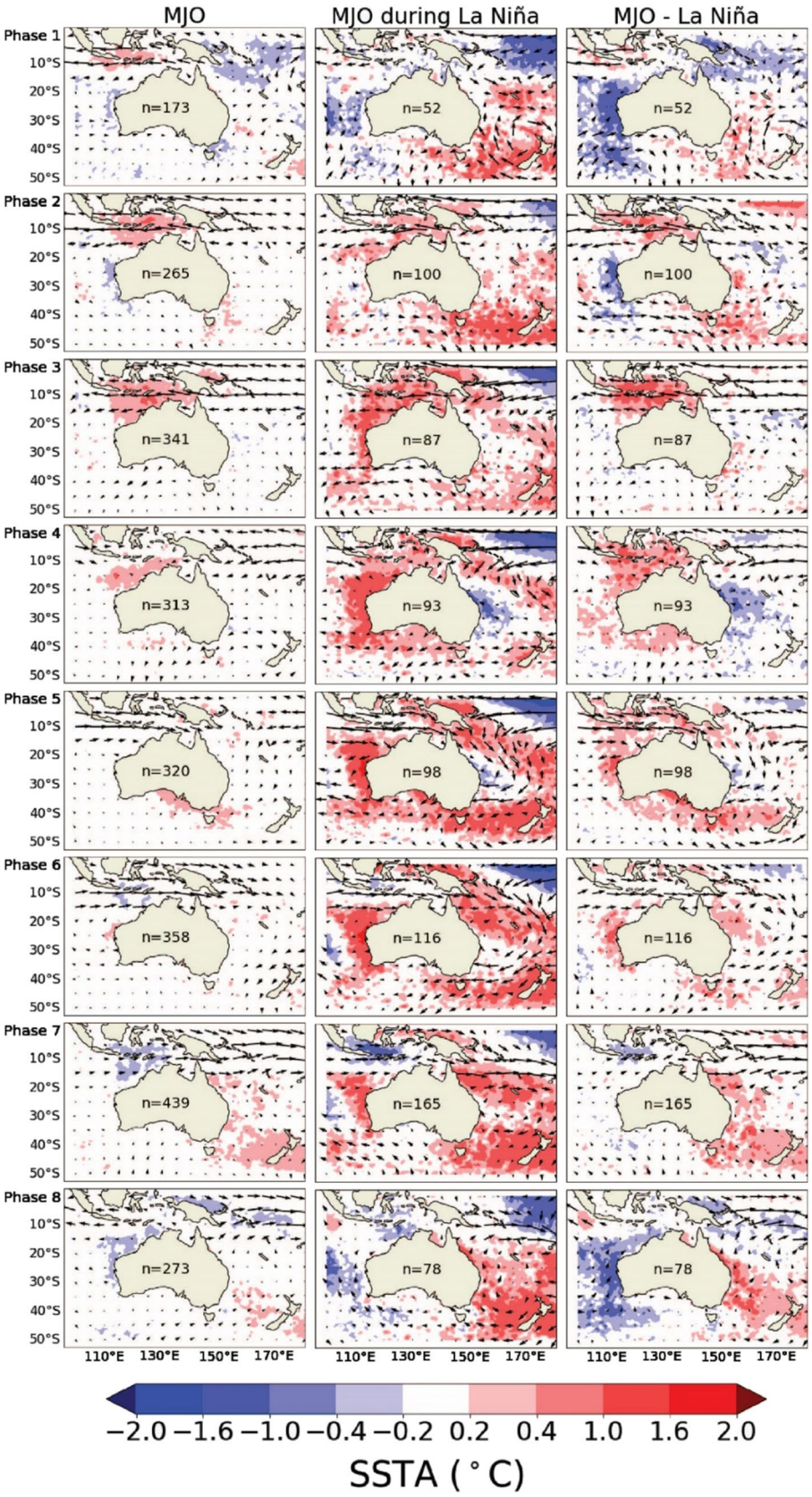

Fig. 15 Composite maps of SST (shaded) and wind (vectors) anomalies with the 8 phases of the MJO during summer (DJF). The left column shows all days in each of the MJO phase, the middle column shows these phases during La Niña periods and the right column shows the same days as the middle column with the average summer La Niña conditions removed. In this way, the right column shows the contribution of the MJO climate variations during La Niña phases

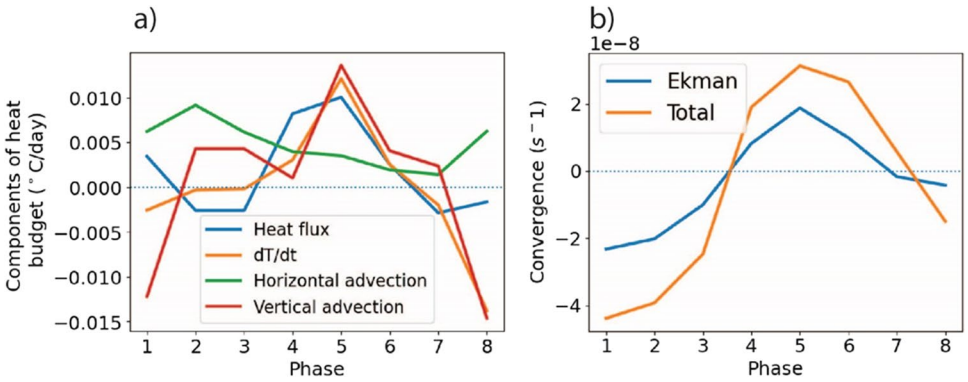

Fig. 16 The composite components of the heat budget analysis performed in the Western Australia region during summer La Niña states, separated by MJO phase, with the average La Niña conditions removed (**a**) and the Ekman and total convergences for the NE Queensland region during the same days (**b**)

4 Discussion and conclusions

In this study, we have highlighted various climate drivers that influence ocean temperatures, including marine heatwaves (MHWs), around Australia on sub-seasonal to seasonal timescales. Understanding the individual effects of climate drivers, and their compounding influences, is crucial for advancing MHW forecasting capabilities.

We analysed connections between drivers and their influences on MHW metrics (occurrence, intensity), and found that drivers with an extended phase duration have a stronger influence on the development of MHWs. As the residence time of any climate mode decreases (i.e., the amount of time a mode spends in a particular phase becomes shorter), the likelihood of this mode to contribute to the occurrence of a MHW also decreases, given that the processes responsible for heat accumulation in a given region tend to be shorter-lived. From Fig. 3 we can see that the phase durations of the ONI are the longest, followed by the IOD, SAM and finally the shortest phase durations can be seen with the STRH, and from Figs. 4, 5, 6, 7, 8, 9, 10, and 11 we see the corresponding decrease in the connection between SST anomalies and MHW hazard ratings in the same order. This can also be seen in the maps showing the correlations between driver indices and positive SST anomalies (Fig. 14, Supplementary Figs. 1–2), as the correlation between seasonal drivers, such as La Niña, remain significant for longer as compared to drivers with higher variability, such as the STRH and the MJO, which lose their significant influence after several weeks (Supplementary Figs. 1–2).

The spatial patterns of MHW hazard rating more closely resemble those of SST anomalies in ENSO (Figs. 4 and 5) than those associated with the sub-seasonal drivers- SAM (Figs. 8 and 9), the STRH (Figs. 10 and 11) and the MJO (Figs. 12 and 13). These results were insensitive to the index type selected, as a variety of daily Niño indices showed very similar results (not shown). During La Niña, positive SST anomalies in the northeast of Australia and down Australia's west coast significantly contribute to MHWs in this region (Figs. 4 and 5). The impact of this heating in the northeast region during summer is less dramatic, as the warming remains offshore. The negative IOD phase is also a strong influence on the formation of MHWs along the Northwest Shelf during winter and spring, when the absence of the Australian monsoon allows the IOD to dominate. The positive SAM phase was the leading driver of warming in the Tasman Sea, presenting a higher-than-average MHW hazard in most seasons (Fig. 9). However, the positive phase of SAM is shown to have the strongest correlation in this region during the spring (Fig. 14), when there is a higher likelihood of positive SAM events (Silvestri and Vera 2009), improving statistical significance. The limited impact of the STRH on MHW hazard (Fig. 11) is likely due to the short lived nature of this atmospheric driver limiting its ability to accumulate sufficient heat in the ocean for a MHW event to occur.

We have attempted to isolate each of the drivers using regression analysis to show their individual contribution to SST variability. However, it should be noted that this technique may not necessarily remove all the influence of other drivers. There is a significant correlation between the positive phase of SAM and La Niña (Table 1), for example, and we can see patterns of increased SST anomalies in the NE QLD region during the positive phase of SAM (Fig. 8 left column), which are more likely due to warming patterns in this region associated with La Niña (Fig. 4 right column).

We also assessed the collective influence of these drivers in the same region and their role in the occurrences of MHWs around Australia. Our findings indicate that, although the MJO does not exhibit a strong link with MHWs alone (Fig. 13), its modulation of the La Niña signal becomes influential in the evolution of MHWs through Ekman transport, upwelling, and heat advection. Particularly when these oceanic conditions are preconditioned by La Niña, the MJO's influence on tropical winds plays a pivotal role. While we highlight the MJO's potential to compound warming along both the east and west coasts of Australia, it is important to acknowledge that the background ENSO state remains dominant. Our results do not indicate that the MJO has the capacity to fundamentally change the overall seasonal MHWs associated with La Niña events, but

instead that the MJO can modulate the background influence of ENSO on regional MHWs on sub-seasonal timescales.

We have introduced a simple MHW hazard index in this study, based on the average weekly excess heat exposure associated with MHWs during each season and considering different phases of various drivers. However, it is important to note that translating this hazard index into a comprehensive risk assessment for marine species and ecosystems requires careful consideration of species-specific factors, including their exposure and vulnerability. For example, a MHW on a coral reef may have very different impacts on the various species that make up the reef ecosystem, depending on the species as well as the timing, duration, and intensity of the heatwave. A MHW occurring in the northern Australian coral reef regions during winter may not have significant impacts if the actual temperature does not exceed the thermal maximum of species of the region. On the other hand, a MHW occurring during a period of high biological productivity, such as during a breeding season or a major migration, may have more severe impacts on a species, regardless of the actual maximum temperature (Barbeaux et al. 2020; Gabriele et al. 2022).

Across the Australian region, we observed strong influences on SST variability by at least one of the examined drivers. However, an interesting exception was identified in the EAC region, with Fig. 14 illustrating that none of the drivers exhibited statistically significant correlations to daily SST anomalies in this region in any season. Although we did not find any significant driver of SST anomalies in this region, our MHW hazard index indicates that during periods of declining El Niño in autumn, the EAC region is at a very high or extreme MHW hazard level (Fig. 5e). This result suggests that SST variability in the EAC region may be due to other processes such as local forcing due to current/wind driven upwelling/downwelling (Roughan and Middleton 2004; Schaeffer and Roughan 2017), the propagation of meanders and frontal eddies (Schaeffer et al. 2017), or remote forcing from Rossby waves (Holbrook and Bindoff 1999; Li et al. 2020).

The Northwest Shelf region exhibits a pronounced temperature transition from cooler spring to warmer summer conditions, which often extends into the austral autumn months (Zhang et al. 2017). We have seen that during this transition phase, there is the potential for several drivers to contribute to increased warming in this region. We observe elevated warming during the decline of El Niño in autumn and winter (Figs. 4 and 5), during the negative phase of the IOD (Fig. 6) and corresponding to MJO phases 2 and 3 (Fig. 13). Figure 14 illustrates this further, as the maps of the leading drivers reveal a scenario in which multiple drivers compete for dominance as the most influential during the summer, autumn, and winter seasons. While both a declining El Niño and the negative phase of the IOD can each contribute to significant warming along the Northwest Shelf, the simultaneous occurrence of these phases is rare (Fig. 3). Nevertheless, these phases have coincided in the past, contributing to the development of intense MHWs in northern Australia during 2015–16 (Benthuysen et al. 2018).

Understanding which drivers decrease the likelihood or intensity of MHWs is also essential for managers to identify favourable conditions that could be used strategically for ecosystem management, fisheries, aquaculture, and other marine resource-related activities. Our analysis has indicated several drivers can reduce the likelihood of MHWs. These include El Niño on Australia's west coast during summer and autumn (Fig. 4c, e) and in the northeast region during spring (Fig. 4b), the positive IOD on the Northwest Shelf during all seasons (Fig. 6), the negative SAM on the Tasman Sea during spring and summer (Fig. 8b, d), and the positive STRH on the Queensland region during spring and summer (Fig. 10a, c).

Our focus has been on presenting results that hold both statistical significance and real-world applicability. However, due to constraints in space, we have intentionally refrained from discussing here the underlying physical mechanisms in detail. This paper serves to lay the groundwork upon which future research can build, such as exploring the more intricate details of the dynamical relationships between drivers and their combined influences including teleconnections and subsurface MHWs.

Overall, our research contributes to a broader understanding of the intricate interplay between climate drivers and their influence on warm ocean temperature extremes, including MHWs, in the Australian region. By scrutinizing the influences of individual drivers and assessing their combined effects, our study underscores the critical need to comprehend the complexity of interactions occurring on shorter timescales within the atmosphere–ocean system.

Supplementary Information The online version contains supplementary material available at https://doi.org/10.1007/s00382-024-07226-x.

Acknowledgements We would like the thank the reviewers for their helpful comments that were essential to improve the manuscript to its final form.

AGM and CMS would like to acknowledge support from the Australian Bureau of Meteorology.

We would like to acknowledge computational support from Australia's National Computational Infrastructure (NCI) and the CLEX Computational Modelling Support (CMS) team. We would also like to thank CLEX graphic designer Georgina Harmer for her assistance with the driver schematic.

Author contributions All authors contributed to the study conception and design. Catherine Gregory analyzed the data and made the figures. The first draft of the manuscript was written by Catherine Gregory and all authors commented on previous versions of the manuscript. All authors read and approved the final manuscript.

Funding Open Access funding enabled and organized by CAUL and its Member Institutions. CHG was supported by an ARC Centre of Excellence for Climate Extremes (CLEX) PhD scholarship, and additional

top-up support from the joint CSIRO-UTAS Quantitative Marine Science program and the Australian Bureau of Meteorology.

NJH was supported by funding from the ARC Centre of Excellence for Climate Extremes (CE170100023) and the National Environmental Science Program Climate Systems Hub.

Data availability All datasets used in this study are open-source and available to be downloaded online.

The OISST v2, NOAA OLR, and NCEP/NCAR datasets were provided by the NOAA/OAR/ESRL PSL, Boulder, Colorado, USA, via their website at https://psl.noaa.gov/

The BRAN202 dataset is publicly available at https://dapds00.nci.org.au/thredds/catalog/gb6/BRAN/catalog.html

Code availability MHW event statistics were computed using the xarray python module (https://github.com/coecms/xmhw), based on the original marine heatwave module (http://github.com/ecjoliver/marineHeatWaves).

Declarations

Competing of interest The authors declare that there are no known competing interests, whether personal, professional, or financial, that would influence the findings of this paper.

References

Allan RJ, Pariwono JI (1990) Ocean-atmosphere interactions in low-latitude Australasia. Int J Climatol 10:145–178

Arias-Ortiz A, Serrano O, Masqué P, Lavery PS, Mueller U, Kendrick GA, Rozaimi M, Esteban A, Fourqurean JW, Marbà N (2018) A marine heatwave drives massive losses from the world's largest seagrass carbon stocks. Nat Clim Chang 8:338

Banzon V, Smith TM, Chin TM, Liu C, Hankins W (2016) A long-term record of blended satellite and in situ sea-surface temperature for climate monitoring, modeling and environmental studies. Earth Syst Sci Data 8:165–176

Barbeaux SJ, Holsman K, Zador S (2020) Marine heatwave stress test of ecosystem-based fisheries management in the Gulf of Alaska Pacific cod fishery. Front Mar Sci 7:703

Barnston AG (1997) Documentation of a highly ENSO-related SST region in the equatorial Pacific. Atmos Ocean 35:367–383

Benthuysen JA, Oliver ECJ, Feng M, Marshall AG (2018) Extreme marine warming across tropical Australia during Austral summer 2015–2016. J Geophys Res Oceans 123:1301–1326

Benthuysen JA, Smith GA, Spillman CM, Steinberg CR (2021) Subseasonal prediction of the 2020 Great Barrier Reef and Coral Sea marine heatwave. Environ Res Lett 16:124050

Cai W, Shi G, Cowan T, Bi D, Ribbe J (2005) The response of the Southern Annular Mode, the East Australian Current, and the southern mid-latitude ocean circulation to global warming. Geophys Res Lett 32(23). https://doi.org/10.1029/2005GL024701

Caputi N, Kangas M, Chandrapavan A, Hart A, Feng M, Marin M, Lestang SD (2019) Factors affecting the recovery of invertebrate stocks from the 2011 Western Australian Extreme Marine Heatwave. Front Mar Sci 6:484

Chamberlain MA, Oke PR, Fiedler RaS, Beggs HM, Brassington GB, Divakaran P (2021) Next generation of Bluelink ocean reanalysis with multiscale data assimilation: BRAN2020. Earth Syst Sci Data 13:5663–5688

Dufek AS, Ambrizzi T, Da Rocha RP (2008) Are reanalysis data useful for calculating climate indices over South America? Ann N Y Acad Sci 1146:87–104

Feng M, Meyers G, Pearce A, Wijffels S (2003) Annual and interannual variations of the Leeuwin Current at 32 S. J Geophys Res Oceans 108(C11). https://doi.org/10.1029/2002JC001763

Gabriele CM, Amundson CL, Neilson JL, Straley JM, Baker CS, Danielson SL (2022) Sharp decline in humpback whale (Megaptera novaeangliae) survival and reproductive success in southeastern Alaska during and after the 2014–2016 Northeast Pacific marine heatwave. Mamm Biol 2(4):1113–1131

Game ET, Watts ME, Wooldridge S, Possingham HP (2008) Planning for persistence in marine reserves: a question of catastrophic importance. Ecol Appl 18:670–680

Gong D, Wang S (1999) Definition of Antarctic oscillation index. Geophys Res Lett 26:459–462

Gregory CH, Holbrook NJ, Marshall AG, Spillman CM (2023) Atmospheric drivers of Tasman sea marine heatwaves. J Clim 36(5):5197–5214

Hendon HH, Salby ML (1994) The life cycle of the Madden–Julian oscillation. J Atmos Sci 51:2225–2237

Hendon HH, Liebmann B, Glick JD (1998) Oceanic Kelvin Waves and the Madden–Julian Oscillation. J Atmos Sci 55:88–101

Hobday AJ, Alexander LV, Perkins SE, Smale DA, Straub SC, Oliver ECJ, Benthuysen JA, Burrows MT, Donat MG, Feng M, Holbrook NJ, Moore PJ, Scannell HA, Sen Gupta A, Wernberg T (2016) A hierarchical approach to defining marine heatwaves. Prog Oceanogr 141:227–238

Holbrook NJ, Bindoff NL (1999) Seasonal temperature variability in the upper southwest Pacific Ocean. J Phys Oceanogr 29:366–381

Holbrook NJ, Scannell HA, Sen Gupta A, Benthuysen JA, Feng M, Oliver ECJ, Alexander LV, Burrows MT, Donat MG, Hobday AJ, Moore PJ, Perkins-Kirkpatrick SE, Smale DA, Straub SC, Wernberg T (2019) A global assessment of marine heatwaves and their drivers. Nat Commun 10:2624

Holbrook NJ, Sen Gupta A, Oliver ECJ, Hobday AJ, Benthuysen JA, Scannell HA, Smale DA, Wernberg T (2020) Keeping pace with marine heatwaves. Nat Rev Earth Environ 1:482–493

Huang Z, Feng M (2021) MJO induced diurnal sea surface temperature variations off the northwest shelf of Australia observed from Himawari geostationary satellite. Deep Sea Res Part II 183:104925

Huang B, Liu C, Freeman E, Graham G, Smith T, Zhang H-M (2021) Assessment and intercomparison of NOAA daily optimum interpolation sea surface temperature (DOISST) version 2.1. J Clim 34:7421–7441

Huang Z, Feng M, Dalton SJ, Carroll AG (2024) Marine heatwaves in the Great Barrier Reef and Coral Sea: their mechanisms and impacts on shallow and mesophotic coral ecosystems. Sci Total Environ 908:168063

Hudson D, Marshall A, Alves O (2011) Intraseasonal forecasting of the 2009 summer and winter Australian heat waves using POAMA. Weather Forecast 26:257–279

Kanamitsu M, Ebisuzaki W, Woollen J, Yang S-K, Hnilo JJ, Fiorino M, Potter GL (2002) NCEP–DOE AMIP-II Reanalysis (R-2). Bull Am Meteor Soc 83:1631–1644

Kobayashi S, Ota Y, Harada Y, Ebita A, Moriya M, Onoda H, Onogi K, Kamahori H, Kobayashi C, Endo H (2015) The JRA-55 reanalysis: general specifications and basic characteristics. J Meteorol Soc Jpn Ser II 93:5-48

Lenssen NJL, Goddard L, Mason S (2020) Seasonal forecast skill of ENSO teleconnection maps. Weather Forecast 35:2387–2406

Li Z, Holbrook NJ, Zhang X, Oliver ECJ, Cougnon EA (2020) Remote forcing of Tasman sea marine heatwaves. J Clim 33:5337–5354

Liebmann B, Smith CA (1996) Description of a complete (interpolated) outgoing longwave radiation dataset. Bull Am Meteor Soc 77:1275–1277

Lim E-P, Hendon HH, Butler AH, Thompson DWJ, Lawrence ZD, Scaife AA, Shepherd TG, Polichtchouk I, Nakamura H, Kobayashi C, Comer R, Coy L, Dowdy A, Garreaud RD, Newman PA, Wang G (2021) The 2019 southern hemisphere stratospheric polar vortex weakening and its impacts. Bull Am Meteor Soc 102:E1150–E1171

Loschnigg J, Meehl GA, Webster PJ, Arblaster JM, Compo GP (2003) The Asian Monsoon, the tropospheric biennial oscillation, and the Indian ocean zonal mode in the NCAR CSM. J Clim 16:1617–1642

Luo J-J, Zhang R, Behera SK, Masumoto Y, Jin F-F, Lukas R, Yamagata T (2010) Interaction between El Nino and extreme Indian ocean dipole. J Clim 23:726–742

Madden RA, Julian PR (1971) Detection of a 40–50 day oscillation in the zonal wind in the tropical Pacific. J Atmos Sci 28:702–708

Maggiorano A, Feng M, Wang XH, Ritchie L, Stark C, Colberg F, Greenwood J (2021) Hydrodynamic drivers of the 2013 marine heatwave on the north west shelf of Australia. J Geophys Res Oceans 126:e2020JC016495

Marshall A, Hendon H (2014) Impacts of the MJO in the Indian Ocean and on the Western Australian coast. Clim Dyn 42:579–595

Marshall A, Hudson D, Wheeler M, Alves O, Hendon H, Pook M, Risbey J (2014) Intra-seasonal drivers of extreme heat over Australia in observations and POAMA-2. Clim Dyn 43:1915–1937

Marshall AG, Hendon HH, Feng M, Schiller A (2015) Initiation and amplification of the Ningaloo Niño. Clim Dyn 45:2367–2385

Marshall AG, Wang G, Hendon HH, Lin H (2023) Madden–Julian Oscillation teleconnections to Australian springtime temperature extremes and their prediction in ACCESS-S1. Clim Dyn 61:431–447

Mcgowan H, Theobald A (2017) ENSO weather and coral bleaching on the Great Barrier Reef, Australia. Geophys Res Lett 44:10,601–10,607

Mckay RC, Boschat G, Rudeva I, Pepler A, Purich A, Dowdy A, Hope P, Gillett ZE, Rauniyar S (2023) Can southern Australian rainfall decline be explained? A review of possible drivers. Wires Clim Change 14:e820

Min S-K, Cai W, Whetton P (2013) Influence of climate variability on seasonal extremes over Australia. J Geophys Res Atmos 118:643–654

Nicholls N (1989) Sea surface temperatures and Australian winter rainfall. J Clim 2:965–973

Nuncio M, Yuan X (2015) The influence of the Indian Ocean dipole on Antarctic sea ice. J Clim 28:2682–2690

Oke PR, Griffin DA, Schiller A, Matear RJ, Fiedler R, Mansbridge J, Lenton A, Cahill M, Chamberlain MA, Ridgway K (2013) Evaluation of a near-global eddy-resolving ocean model. Geosci Model Dev 6:591–615

Oliver ECJ, Donat MG, Burrows MT, Moore PJ, Smale DA, Alexander LV, Benthuysen JA, Feng M, Sen Gupta A, Hobday AJ, Holbrook NJ, Perkins-Kirkpatrick SE, Scannell HA, Straub SC, Wernberg T (2018a) Longer and more frequent marine heatwaves over the past century. Nat Commun 9:1324

Oliver ECJ, Perkins-Kirkpatrick SE, Holbrook NJ, Bindoff NL (2018b) Anthropogenic and natural influences on record 2016 marine heat waves. Bull Am Meteor Soc 99:S44–S48

Oliver E, Thompson K (2010) Madden-Julian Oscillation and sea level: local and remote forcing. J Geophys Res 115

Pearce AF, Lenanton R, Jackson G, Moore J, Feng M, Gaughan D (2011) The "marine heat wave" off Western Australia during the summer of 2010/11. Western Australian Fisheries and Marine Research Laboratories

Philander SGH (1983) El Niño Southern Oscillation phenomena. Nature 302:295-301

Reynolds RW, Smith TM, Liu C, Chelton DB, Casey KS, Schlax MG (2007) Daily high-resolution-blended analyses for sea surface temperature. J Clim 20:5473–5496

Risbey JS, Pook MJ, Mcintosh PC, Wheeler MC, Hendon HH (2009) On the remote drivers of rainfall variability in Australia. Mon Weather Rev 137:3233–3253

Roemmich D, Gilson J, Davis R, Sutton P, Wijffels S, Riser S (2007) Decadal spinup of the South Pacific subtropical gyre. J Phys Oceanogr 37:162–173

Roughan M, Middleton JH (2004) On the East Australian current: variability, encroachment, and upwelling. J Geophys Res Oceans 109

Saji N, Goswami BN, Vinayachandran P, Yamagata T (1999) A dipole mode in the tropical Indian Ocean. Nature 401:360–363

Schaeffer A, Roughan M (2017) Subsurface intensification of marine heatwaves off southeastern Australia: the role of stratification and local winds. Geophys Res Lett 44:5025–5033

Schaeffer A, Gramoulle A, Roughan M, Mantovanelli A (2017) Characterizing frontal eddies along the East Australian Current from HF radar observations. J Geophys Res Oceans 122:3964–3980

Silvestri G, Vera C (2009) Nonstationary impacts of the southern annular mode on Southern Hemisphere climate. J Clim 22:6142–6148

Smale DA, Wernberg T, Oliver ECJ, Thomsen M, Harvey BP, Straub SC, Burrows MT, Alexander LV, Benthuysen JA, Donat MG, Feng M, Hobday AJ, Holbrook NJ, Perkins-Kirkpatrick SE, Scannell HA, Sen Gupta A, Payne BL, Moore PJ (2019) Marine heatwaves threaten global biodiversity and the provision of ecosystem services. Nat Clim Chang 9:306–312

Smith KE, Burrows MT, Hobday AJ, Sen Gupta A, Moore PJ, Thomsen M, Wernberg T, Smale DA (2021) Socioeconomic impacts of marine heatwaves: Global issues and opportunities. Science 374:eabj3593

Speer MS, Leslie LM, Fierro AO (2011) Australian east coast rainfall decline related to large scale climate drivers. Clim Dyn 36:1419–1429

Spillman CM, Hobday AJ (2014) Dynamical seasonal ocean forecasts to aid salmon farm management in a climate hotspot. Clim Risk Manag 1:25–38

Student, (1908) The probable error of a mean. Biometrika 6:1–25

Stuecker MF, Timmermann A, Jin F-F, Chikamoto Y, Zhang W, Wittenberg AT, Widiasih E, Zhao S (2017) Revisiting ENSO/Indian Ocean Dipole phase relationships. Geophys Res Lett 44:2481–2492

Talley LD, Pickard GL, Emery WJ, Swift JH (2011) Chapter 7 - dynamical processes for descriptive ocean circulation. In: Talley LD, Pickard GL, Emery WJ, Swift JH (eds) Descriptive physical oceanography (Sixth Edition). Academic Press, Boston, pp 187–221

Tozuka T, Feng M, Han W, Kido S, Zhang L (2021) 8 - The Ningaloo Niño/Niña: Mechanisms, relation with other climate modes and impacts. In: Behera SK (ed) Tropical and extratropical air-sea interactions. Elsevier, pp 207–219

Virts KS, Wallace JM (2014) Observations of temperature, wind, cirrus, and trace gases in the tropical tropopause transition layer during the MJO. J Atmos Sci 71:1143–1157

Vitart F, Ardilouze C, Bonet A, Brookshaw A, Chen M, Codorean C, Déqué M, Ferranti L, Fucile E, Fuentes M, Hendon H, Hodgson J, Kang HS, Kumar A, Lin H, Liu G, Liu X, Malguzzi P, Mallas I, Manoussakis M, Mastrangelo D, Maclachlan C, Mclean P, Minami A, Mladek R, Nakazawa T, Najm S, Nie Y, Rixen M, Robertson AW, Ruti P, Sun C, Takaya Y, Tolstykh M, Venuti F, Waliser D, Woolnough S, Wu T, Won DJ, Xiao H, Zaripov R, Zhang L (2017) The subseasonal to seasonal (S2S) prediction project database. Bull Am Meteorol Soc 98:163–173

Wallace JM, Rasmusson EM, Mitchell TP, Kousky VE, Sarachik ES, Von Storch H (1998) On the structure and evolution of ENSO-related climate variability in the tropical Pacific: lessons from TOGA. J Geophys Res Oceans 103:14241–14259

Wang S-Y, L'heureux M, Chia H-H (2012) ENSO prediction one year in advance using western North Pacific sea surface temperatures. Geophys Res Lett 39

Wang Y, Holbrook NJ, Kajtar JB (2023) Predictability of marine heatwaves off Western Australia using a linear inverse model. J Clim 1–40

Wang G, Hendon HH (2020) Impacts of the Madden–Julian Oscillation on wintertime Australian minimum temperatures and Southern Hemisphere circulation. Clim Dyn 55:3087–3099

Weller RA, Anderson SP (1996) Surface meteorology and air-sea fluxes in the western equatorial Pacific warm pool during the TOGA coupled ocean-atmosphere response experiment. J Clim 9:1959–1990

Werner A, Maharaj AM, Holbrook NJ (2012) A new method for extracting the ENSO-independent Indian Ocean Dipole: application to Australian region tropical cyclone counts. Clim Dyn 38:2503–2511

Wheeler MC, Hendon HH (2004) An all-season real-time multivariate MJO index: Development of an index for monitoring and prediction. Mon Weather Rev 132:1917–1932

White CJ, Domeisen DIV, Acharya N, Adefisan EA, Anderson ML, Aura S, Balogun AA, Bertram D, Bluhm S, Brayshaw DJ, Browell J, Büeler D, Charlton-Perez A, Chourio X, Christel I, Coelho CaS, Deflorio MJ, Delle Monache L, Di Giuseppe F, García-Solórzano AM, Gibson PB, Goddard L, González Romero C, Graham RJ, Graham RM, Grams CM, Halford A, Huang WTK, Jensen K, Kilavi M, Lawal KA, Lee RW, Macleod D, Manrique-Suñén A, Martins ESPR, Maxwell CJ, Merryfield WJ, Muñoz ÁG, Olaniyan E, Otieno G, Oyedepo JA, Palma L, Pechlivanidis IG, Pons D, Ralph FM, Reis DS, Remenyi TA, Risbey JS, Robertson DJC, Robertson AW, Smith S, Soret A, Sun T, Todd MC, Tozer CR, Vasconcelos FC, Vigo I, Waliser DE, Wetterhall F, Wilson RG (2022) Advances in the application and utility of subseasonal-to-seasonal predictions. Bull Am Meteorol Soc 103:E1448-E1472

Xu J, Lowe RJ, Ivey GN, Jones NL, Zhang Z (2018) Contrasting heat budget dynamics during two la niña marine heat wave events along Northwestern Australia. J Geophys Res Oceans 123:1563–1581

Zangvil A (1975) Temporal and spatial behavior of large-scale disturbances in tropical cloudiness deduced from satellite brightness data. Mon Wea Rev 103:904–920

Zhang N, Feng M, Hendon HH, Hobday AJ, Zinke J (2017) Opposite polarities of ENSO drive distinct patterns of coral bleaching potentials in the southeast Indian Ocean. Sci Rep 7:2443

Zhao S, Jin F-F, Stuecker MF (2019) Improved predictability of the Indian Ocean Dipole using seasonally modulated ENSO Forcing Forecasts. Geophys Res Lett 46:9980–9990